Journal of Applied Biology & Biotechnology Vol. 11(5), pp. 174-197, Sep-Oct, 2023
Available online at http://www.jabonline.in
DOI: 10.7324/JABB.2023.11521

Evaluating the anti-inflammatory potential of *Mesua ferrea* linn. stem bark through network pharmacology approach

Jyothsna Kalyana Sundaram[1], Manjunatha Hanumanthappa[2]*, Shivananada Kandagalla[3], Sharath Belenahalli Shekarappa[4], Pavan Gollapalli[5], Umme Hani[1]

[1]Department of PG Studies and Research in Biotechnology, Kuvempu University, Shankaraghatta, Karnataka, India.
[2]Department of Biochemistry, Bengaluru University, Bengaluru, Karnataka, India.
[3]Laboratory of Computational Modeling of Drugs, Higher Medical and Biological School, South Ural State University, Chelyabinsk, Russia.
[4]Department of Bioinformatics and Life Science, Soongsil University, Seoul - 06978, South Korea.
[5]Center for Bioinformatics and Biostatistics, Nitte (Deemed to be University), Mangaluru, Karnataka, India.

ARTICLE INFO

Article history:
Received on: March 16, 2023
Accepted on: June 30, 2023
Available online: August 10, 2023

Key words:
Mesua ferrea,
Network pharmacology,
Gene ontology,
Molecular docking,
MD simulation.

ABSTRACT

Mesua ferrea Linn. (MF) is a medicinal plant whose stem bark has historically been used to treat skin disorders, gastrointestinal, and anti-inflammatory conditions. Although the MF stem bark's contribution to inflammation was assessed, its exact mode of action remained unknown. This study aimed to investigate the pharmacological mechanisms of MF against inflammation utilizing network pharmacology, molecular docking, and molecular dynamics (MD) simulation. An integrated network pharmacology approach was used to predict the pharmacological basis and potential mechanisms by which these ingredients may treat and prevent inflammation. This approach included target identification, network construction, topological analysis, gene ontology and Kyoto Encyclopedia of Genes and Genomes pathway enrichment analysis, molecular docking, and MD simulation. Utilizing the pre- Absorption, Distribution, Metabolism, Elimination, and Toxicity tool, the drug-likeness of the phytoconstituents was evaluated. Protein-protein interaction network and protein interaction network was constructed. The results indicated that androgen receptor, Estrogen Receptor alpha, CYP19A1, retinoic acid receptor alpha, nuclear factor erythroid 2-related factor 2, thyrotropin receptor, nuclear factor kappa B subunit 1, and Albumin are crucial proteins engaged directly or indirectly in inflammatory pathways and illnesses. Finally, the targets are validated by molecular docking and MD simulation. MF may be effective for alleviating inflammatory conditions and the mechanism of action is characterized by multi-compound, multi-target, and multi-pathways. Thus, our study provides certain evidence for the development and utilization of medicinal plants.

1. INTRODUCTION

Inflammation is a normal, robust physiological process mediated by various signaling molecules from leukocytes, macrophages, and mast cells. It can also be viewed as a complex system that senses and resolves homeostatic perturbations initiated within the body or outside. It is the central communication network and regulatory process that senses and controls threats, damage, and healing [1]. To prevent inflammation, several types of synthetic and phytochemical anti-inflammatory agents are used. Usually, the anti-inflammatory agents in clinical use exhibit certain properties such as analgesic and antipyretic properties along with ulcerogenicity and impairment of blood clotting as a side effect. These effects can be mitigated by using secondary metabolites from medicinal plants. The anti-inflammatory therapeutic efficacy of the medicinal plant is extensively used in the Indian system of medicine. Natural products have indeed been important in medicine because of their potential to bind and regulate the cellular targets involved in disease. Several bioactive scaffolds are present in medicinal plants that can be used to treat a wide range of diseases [2].

Network pharmacology, an *in-silico* method that blends systematic medicine with information science, is becoming a new frontier in drug discovery and development [3]. *In-silico* methods assist in quickly predicting the behavior of a large number of chemicals in a high-throughput mode, based on the compound structure before its synthesis. In the process of developing natural drugs, the computational investigation is utilized to not only identify novel targets and novel compounds with high affinities for respective targets but also to determine the metabolic pathways of active molecules [4]. Network pharmacology helps to predict active ingredients and mechanisms of action by integrating drugs and diseases into biomolecular networks. The network emphasizes the relationships between proteins, so it is

*Corresponding Author:
Manjunatha Hanumanthappa,
Department of Biochemistry, Bengaluru University,
Bengaluru - 560 056, Karnataka, India.
E-mail: manjunatha75 @ gmail.com

possible to suggest pairs or groups of drug targets that might work well together to treat or overcome the disease.

Mesua ferrea Linn. (MF), commonly known as Nagkesar, belongs to the family *Clusiaceae* (Guttiferae). Conventionally, the stem bark of MF was used to treat various ailments, including asthma, cough, dyspepsia, fever, headache, piles, itchiness, ulcers, and stomachic disorders. Scientific studies such as anti-inflammatory, anti-gastric, anti-bacterial, and anti-oxidant activities, etc., have confirmed the traditional importance of MF [5,6]. Keawsa-Ard *et al*. reported the isolation of the bioactive compounds from the MF stem part, confirmed antibacterial activity against *Staphylococcus aurens,* and anticancer activity against MCF-7 and NCI-H187 cell lines [7]. The immunomodulatory activity of mesuol from MF flower was studied by [8]. Chanda *et al*. demonstrated the antibacterial and antifungal activity of MF seed extract using different polar solvents [9]. The antibacterial efficacy of the methanol extract of whole flowers of MF was found against various strains of bacteria [10]. The *in-vivo* anti-inflammatory activities were analyzed using 80% ethanol stem bark extract of MF regarding the inhibition of paw edema [11]. Asif *et al*. studied the molecular mechanisms responsible for *in-vitro* apoptotic, antimetastatic, and antitumor activities of α-amyrin and betulinic acid bioactive sub-fraction (SF-3) extracted from MF stem bark in human colon cancer HCT 116 cells [12]. The *in-vitro* and *in-vivo* anti-inflammatory activities of MF bark were examined [13], where the ethyl acetate extract showed the inhibition of pro-inflammatory cytokines in LPS-induced RAW 264.7 cells and also inhibitory activities at the late stage of carrageenan-induced paw edema. Most of the *in-vitro* and *in-vivo* studies confirmed that MF stem bark compounds are mainly involved in anti-inflammatory activities. Even though the stem bark of MF has been demonstrated to have anti-inflammatory properties, the mechanism of action remains unknown due to its complexity.

So far, diseases are prevented by using a single inhibitor; sometimes, it becomes difficult to defeat diseases by using only one drug target; under this circumstance, multiple inhibitors can be used to prevent the disease. Nevertheless, it is difficult to understand the molecular mechanism of multiple molecules' action. Hence understanding their complex interactions and functional influence will help to overcome any difficulties. Therefore, the present study aims to systematically investigate the potential protein targets, biological processes, and signaling pathways of MF stem bark phytoconstituents using the network pharmacology approach. For this, initially, the curation of compounds was done by literature survey and using primary databases, and the interactome of the compound was analyzed using a chemical-protein interaction database. The protein interaction network (PIN) was constructed and used for the prediction of mechanisms of molecular action and functional enrichment analysis. Finally, to validate the results, molecular docking and molecular dynamics (MD) simulation was also performed on active compounds and major proteins.

2. MATERIALS AND METHODS

2.1. Collection of Plant Material and Extraction

The stem bark of MF was collected from Thirthahalli, Shivamogga district, Karnataka. The stem bark was cleaned with deionized water, sliced into small pieces, and dried in the shade before being crushed with a mechanical blender. The powdered material was subjected to a sequential type of SOXHLET extraction. About 1 kg of powdered plant material was placed into a soxhlet thimble and extracted for 48 h, sequentially with petroleum ether, chloroform, and ethanol in the order of polarity. Using a rotary flash evaporator, the extract was filtered and concentrated in a vacuum at reduced pressure. The solvent was removed and dried in a desiccator. The dried extract was subjected to a High-resolution liquid chromatograph mass spectrometer (HR-LCMS) analysis.

2.2. HR-LCMS Analysis of Stem Bark Extract

The HR-LCMS G6550A system (Agilent Technologies) was used to investigate the bioactive components of the produced crude ethanolic extract from MF stem bark. Chromatography was done using 30 min ± ESI 10032014_MSMS.m technique and 250°C was the gas temperature used for the analysis. Identification was made using the protonated compound's theoretical mass. The analysis was carried out at the Indian Institute of Technology's sophisticated analytical instrument facility in Mumbai, India. The compounds were identified by comparing the compounds' retention time (RT) and masses to the archived Metlin library kept at IIT, Bombay.

2.3. Compound Retrieval and Structure Prediction Through Primary Databases

Besides the extraction process, a literature survey also retrieved phytoconstituents of MF stem bark from PubMed Central/MEDLINE. NCBI's PubMed Central (https://www.ncbi.nlm.nih.gov/pmc/) is a free online source search engine for retrieving biomedical research literature. For screening of phytoconstituents from the primary databases, we used terms like "*Mesua ferrea*, *Mesua ferrea* stem bark, and inflammation". Overall, 71 articles were obtained, 35 of which were on MF stem bark (the database was accessed from September 22nd, 2018 to November 10th, 2018). The phytoconstituents collected are listed in Table 1a [12,14,15], and their PubChem ID and canonical smiles are listed in Table 1b.

The common compounds of MF stem bark from the extraction process and literature survey were submitted for structure and target prediction using primary databases. Primary databases such as PubChem (https://pubchem.ncbi.nlm.nih.gov/) and ChEMBL (https://www.ebi.ac.uk/chembl/) were used to get chemical structures [16]. The ChemDraw Ultra tool was used to convert their file format from "structure-data file format (.sdf) to mol file format (.mol)" for further studies.

2.4. Toxicity and Biological Activity Prediction

The phytoconstituent's drug-likeness absorption, distribution, metabolism, elimination, and toxicity (ADMET) were evaluated using an open-source pre-ADMET server (https://preadmet.bmdrc.kr/). To confirm a drug-like molecule, Lipinski's rule of five (RO5) was considered, which states that the compound's molecular weight should be ≤500 Daltons, the number of H-donors should be 5, the number of H-acceptors should be 10, and cLog*P* should not be >5. Molinspiration Cheminformatics software (https://www.molinspiration.com/) was used to evaluate the compounds' molecular characteristics and biological activity spectra were predicted using prediction of activity spectra for substances online (http://www.pharmaexpert.ru/passonline/), a tool for assessing the biological potential of drug-like molecules that provides the simultaneous prediction of many biological activities [17]. The biological activities probability of molecules were determined by their activeness and inactiveness value, and are ranging from 0 to 1. Here, we considered the probability of activeness.

2.5. Compound Target Mining

For mining/retrieving the potential targets of compounds, we used different databases viz., (1) PubChem (https://pubchem.

Table 1a: List of stem bark phytoconstituents curated from literature survey using PubMed central (https://www.ncbi.nlm.nih.gov/pmc/).

S. No.	Phytochemical name	Extract	Techniques	PMID/URL
1	• α-Amyrin • (−)-globulol • Phthalic acid mono-2-ethylhexyl ester • (+)-aromadendrene • 2,4-di-tert-butylphenol • Betulinic acid	n-hexane	GC-MS analysis	28807224
2	• Betulinic acid • Mesuabixanthone-A • Mesuabixanthone-B • Pyranojacareubin • Isoeuxanthone • (−)-Epicatechin	Petroleum	IR, ‘H NMR and EIMS	https://doi.org/10.1080/10575639308043837
3	• Spinasterol	Methanol	NMR	http://dx.doi.org/10.6000/1927-5129.2014.10.17

Table 1b: List of compounds with their pubchem Id and canonical smiles (https://pubchem.ncbi.nlm.nih.gov/).

S. No.	Compound names	Pubchem ID	Canonical smiles
MF1	(−)-Epicatechin	72276	C1C(C(OC2=CC(=CC(=C21)O)O)C3=CC(=C(C=C3)O)O)O
MF2	(−)-Globulol	12304985	CC1CCC2C1C3C(C3(C)C)CCC2(C)O
MF3	(+)-Aromadendrene	11095734	CC1CCC2C1C3C(C3(C)C)CCC2=C
MF4	2,4-Di-tert-butylphenol	7311	CC(C)(C)C1=CC(=C(C=C1)O)C(C)(C)C
MF5	α-Amyrin	73170	CC1CCC2(CCC3(C(=CCC4C3(CCC5C4(CCC(C5(C)C)O)C)C)C2C1C)C)C
MF6	Betulinic acid	64971	CC(=C)C1CCC2(C1C3CCC4C5(CCC(C(C5CCC4(C3(CC2)C)C)(C)C)O)C)C(=O)O
MF7	Epiglobulol	11858788	CC1CCC2C1C3C(C3(C)C)CCC2(C)O
MF8	Isoeuxanthone	5493674	C1=CC2=C(C(=C1)O)C(=O)C3=C(O2)C=C(C=C3)O
MF9	Pyranojacareubin	15307925	CC1(C=CC2=CC3=C(C(=C2O1)O)OC4=CC5=C(C=CC(O5)(C)C)C(=C4C3=O)O)C
MF10	Phthalic acid mono-2-ethylhexyl ester	20393	CCCCC(CC)COC(=O)C1=CC=CC=C1C(=O)O
MF11	Spinasterol	5281331	CCC(C=CC(C)C1CCC2C1(CCC3C2=CCC4C3(CCC(C4)O)C)C)C(C)C

ncbi.nlm.nih.gov/) (2) ChEMBL (https://www.ebi.ac.uk/chembl/), Pubchem and chembl are the primary databases that provide information about chemicals and their biological interactions and phenotypic effects. (3) STITCH ver4.0 (http://stitch.embl.de/), aims to integrate the data dispersed over the literature and various databases of biological pathways, drug target interactions, and binding affinities. In which a confidence score of 0.9 was considered to retrieve targets. (4) SwissTargetPrediction (http://www.swisstargetprediction.ch/) a web tool that uses a combination of 2D and 3D measurements by known ligands to predict targets of bioactive molecules, (5) Traditional Chinese medicine systems pharmacology (TCMSP) (https://old.tcmsp-e.com/tcmsp.php), a Chinese herbal medicine database of system pharmacology, provides information regarding relationships between drugs, targets, and diseases and also includes pharmacokinetic properties for natural compounds and (6) Pharmmapper (http://www.lilab-ecust.cn/pharmmapper/), a web-based server used to identify the potential targets for drugs or natural compounds based on pharmacophore mapping approach. From January 10 to March 30, 2019, the databases are evaluated.

2.6. Target Fishing for Inflammation

Inflammation-related targets were retrieved from two sources: (1) GeneCards (https://www.genecards.org/), an integrative database that provides information related to human genes and disease-related genes. (2) Open Targets (https://www.targetvalidation.org/) comprehensive platform, which provides systematic identification and prioritization of potential targets, drugs, and phenotypes. To search for targets related to inflammation, we used the input keywords “*inflammation*” and “*Homo sapiens*” in the above-mentioned human disease databases (the datasets are evaluated between April 20th, 2019, and May 16th, 2019).

2.7. Core Interactome Construction and its Analysis

2.7.1. Compound-target network (C-T network)

The C-T interaction network [Figure 1a] was created using the open-source software Cytoscape v2.8.0, a popular tool for visualizing complex networks and interactions [18] (http://www.cytoscape.org).

For core interactome construction, common targets involved in both the C-T network and disease PPI network were retrieved by constructing a Venn diagram, and the network is called a C-T -disease network (C-T-D network). The common targets interaction network was obtained from the PPIs database STRING v9.1 (https://string-db.org/) [19], which includes both direct and indirect interactions, i.e., physical and functional correlations. Selecting the high confidence/interaction score of 0.7 and interactions of no more than 10. A confidence score, which ranges from 0 to 1, will indicate the predicted probability of important genes. The interactions are used for constructing the PIN using Cytoscape v3.7.1.

2.7.2. Topological analysis of PIN

Topological parameters characterize the quantitative patterns and measures of the nodes and edges. Analysis of topological parameters such as degree distribution, betweenness and closeness centralities,

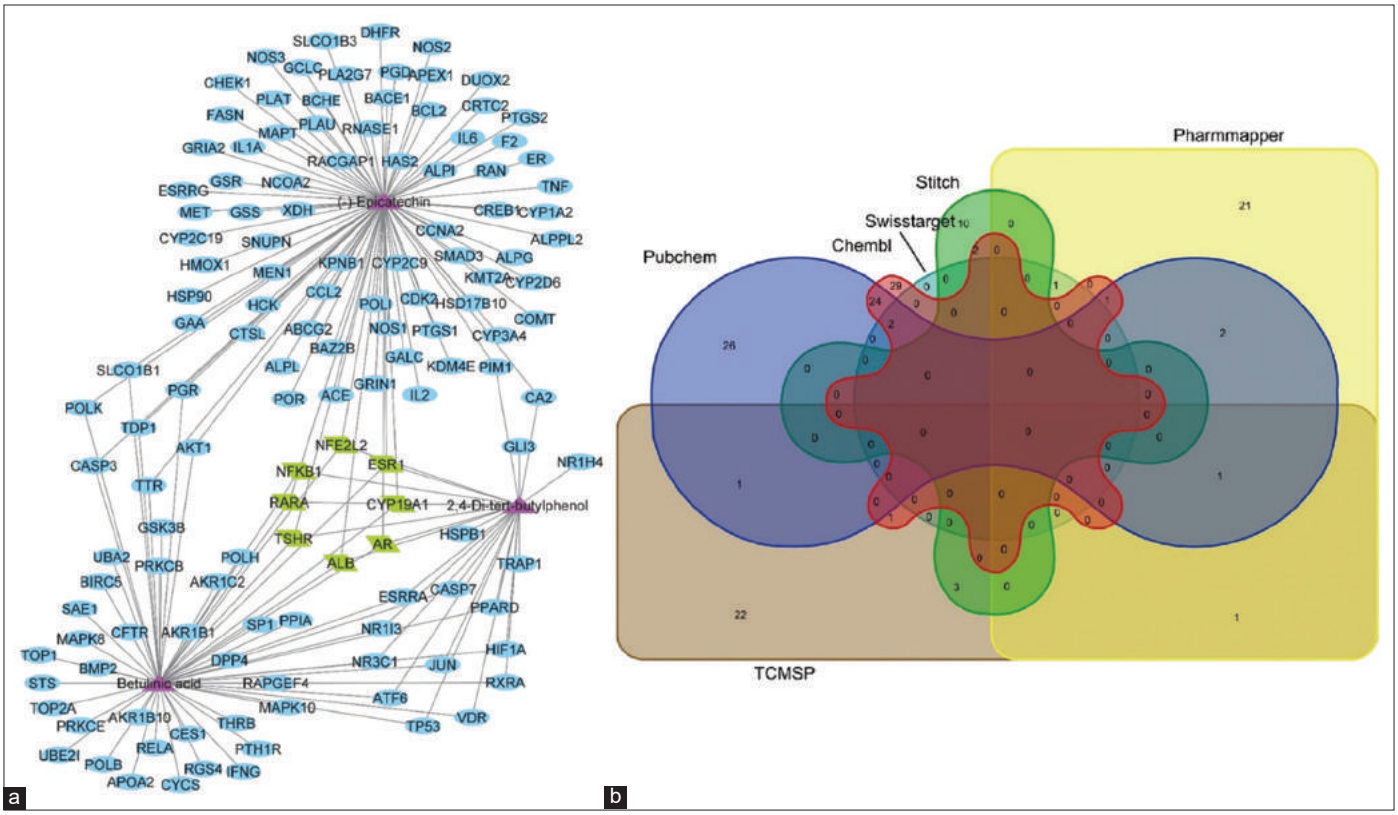

Figure 1: (a) Compound-target interaction network, where purple-colored and triangle shapes are the major compounds. (b) Venn diagram for compounds targets from different databases (Pubchem, Chembl, Stitch, Swisstargetprediction, TCMSP, Pharmmapper).

topological coefficients, shortest pathlength, average clustering coefficient, etc., of directed and undirected networks is analyzed using the Network Analyzer [20], a Cytoscape plug-in, which helps to construct the intersection and union of nodes and edges.

2.7.3. Biological process and pathway enrichment analysis

The backbone network genes were used for gene ontology (GO) biological process and pathway enrichment analysis. The analysis was conducted in the enrichment tool ShinyGO v0.76 (http://bioinformatics.sdstate.edu/go/), a graphical enrichment analysis tool based on multiple R/Bioconductor packages and extensive annotation and pathway datasets generated from many sources [21]. The following parameters were considered for the analyses: species = Human, false discovery rate cutoff = 0.05, and the number of pathways to show = 20.

2.8. Molecular Docking

2.8.1. Ligand preparation

The 2D structures of compounds, namely, MF1, MF4, and MF6, were retrieved from the PubChem database. Diclofenac was used as a standard and its 2D structure was also retrieved. To reduce the overall potential energy of the molecule, energy minimization has to be done. In our study for energy minimization, the ChemBio3D tool was used. The energy-minimized ligand molecules were used as input for AutoDock Vina. AutoDock Vina was used for molecular docking and virtual screening, which employs a powerful gradient optimization algorithm and scoring function [22].

2.8.2. Protein preparation

The 3D structures of target proteins androgen receptor (AR) (PDB ID: 2AMA), estrogen receptor alpha (ESR1) (PDB ID: 1A52), CYP19A1 (PDB ID: 3EQM), retinoic acid receptor alpha (RARA) (PDB ID: 3A9E), nuclear factor erythroid 2 related factor 2 (NFE2L2) (PDB ID: 3ZGC), thyrotropin receptor (TSHR) (PDB ID: 3G04), nuclear factor kappa B subunit 1 (NFKB1) (PDB ID: 1SVC) and Albumin (ALB) (PDB ID: 1H9Z) were retrieved from the RCSB PDB (Protein Data Bank) (https://www.rcsb.org/) online server. Heteroatoms were removed from the receptor. The grid box was set using the MGL tools. The grid box was configured to cover the macromolecule's region of interest. MGL tool is the graphical user interface used for the visualization and analysis of molecular structures. The grid box coordinate values were set with a spacing of 1Å. A maximum of 10 conformers of each ligand were taken into account throughout the docking process. Following docking, complexes 2D and 3D graphical representations were derived using LigPlot^{+} [23] and PyMol educational version (The PyMOL Molecular Graphics System, Version 1.2r3pre, Schrödinger, LLC).

2.9. MD Simulation

MDs simulation was carried out using Groningen machine for chemical simulation (GROMACS) software v2018 (https://www.gromacs.org/). The best-docked ligand-protein complexes were subjected to 100 ns MD simulation by parameterizing using GROMOS94 54a7 force field. The docked complexes, such as ALB-MF6 and RARA-MF1, were solvated in the TIP3P water model with a buffer distance of 10Å in the center and served as a boundary for the simulation box, with periodic boundary conditions. To balance the system's overall charge, Na^{+} and Cl^{-} ions were added. The energy required for each step is reduced by the steepest descents conjugate gradient. The particle mesh Ewald treatment limited the bonding parameters for hydrogen and long-range

electrostatic forces using the SHAKE algorithm. The constant volume (NVT) and constant pressure (NPT) were used to calibrate the system at 300 K for 1000 ps. With a cutoff of 0.10 nm, the Lennard-Jones potentials were created for van der Waals interactions, and the LINCS algorithm was used to constrain the bonds and angles. To assess the results root mean square deviation (RMSD) and root mean square fluctuation (RMSF) was used. The binding free energy of the MF1-RARA and MF6-ALB complexes was assessed using molecular mechanics and generalized born surface area (MM-GBSA) [24,25].

3. RESULTS

3.1. Stembark Extraction and HR-LCMS Analysis

On a sequential type of soxhlet extraction, the maximum percentage yield was obtained for ethanol extract, followed by petroleum ether and chloroform. The high-yield ethanolic extract of stem bark was subjected to HR-LCMS analysis. HR-LCMS results for the sample show molecular formulas $C_{30}H_{48}O_3$, $C_{15}H_{14}O_6$, and $C_{14}H_{22}O$ and molecular weights of 456.69, 290.29, and 206.30, respectively, as shown in Supplementary Table 1. These results demonstrate that the compounds are indeed betulinic acid, (-)-epicatechin, and 2,4-Di-tert-butylphenol because the chromatogram indicates the RT and molecular weight.

3.2. Screening of Compounds

Based on a literature survey, 11 MF stem bark phytoconstituents were screened-out [Table 1a]. On comparing the results of HR-LCMS and literature survey, three common phytoconstituents were found and are highlighted by Aqua color [Table 1b], and structures of these phytoconstituents were retrieved from primary chemical databases, PubChem and chEMBL. The information obtained from the chemical databases would reveal the structural activity relationship of the compounds. The converted file format from ".sdf" to ".mol" is used to evaluate the toxicity of compounds.

3.3. Toxicity Prediction

The primary criterion in determining the nature of a molecule as a medication is 2D structure-based toxicity prediction. It is the initial step toward determining their toxicity *in vivo*. As a result, the compound's drug-likeness should be assessed. Pre-ADMET predicts the drug-like molecule based on Lipinski's RO5, and the compounds MF1 [(-)-Epicatechin], MF4 [2,4-Di-tert-butylphenol] had greater human intestine absorption than MF6 [Betulinic acid]. Nonetheless, all compounds followed RO5. In the meantime, they can enter the skin and bind the plasma protein. Table 2a-d show their molecular characteristics, biological activities, and the likelihood of anti-inflammatory action.

3.4. Target Gene Retrieval of Phytoconstituents

Overall, 147 potential targets for the active compounds were mined from PubChem, ChEMBL, STITCH, Swiss Target Prediction, TCMSP, and Pharmmapper databases and the Venn diagram for retrieved targets was generated using "Venn Diagrams" tool (https://bioinformatics.psb.ugent.be/webtools/Venn/) [Figure 1b]. Targets' Uniprot IDs (https://www.uniprot.org/) are collected and are listed in Table 3a.

3.5. Target Fishing for Inflammation

Open Targets and Gene Cards tools were used to mine inflammation-related targets. We obtained 10025 targets associated with inflammation by combining the targets of two tools. The obtained inflammation-related targets and compound targets were placed in a VennDiagrams tool [Figure 2]. From the Venn diagram, 134 common targets implicated in inflammation are obtained, which were used for PPI development and are included in Table 3b.

3.6. PIN Construction, Screening of Key Targets, and Analysis

The common targets from the Venn diagram are subjected to the STRING database to build a PPI network [Figure 3a] and are visualized in Cytoscape v3.7.1. The interactome is considered the core-interactome, which consists of 133 nodes and 1252 edges with an average node degree of 18.7 [Figure 3b]. From this core-interactome, eight targets AR, ESR1, CYP19A1, RARA, NFE2L2, TSHR, NFKB1, and ALB, are considered key or major targets, which are primary neighbors and have common interaction with the active compounds. The STRING (http://apps.cytoscape.org/apps/stringapp), Cytoscape plugin was used to build an interactive network for key targets and is considered a backbone network [Figure 4]. Both the core-interactome and backbone network was analyzed by Network analyzer, Various parameters, such as Clustering coefficient, Network density, Network centralization, Network heterogeneity, and characteristic path length were calculated and the comparative network topological parameters of the core-interactome and backbone network are presented in Table 4.

In the backbone network AR, ESR1, CYP19A1, RARA, NFE2L2, NFKB1, and ALB form an interactive network, whereas TSHR was independent of the interactive network. Topological parameters viz, Degree, Betweenness centrality, and closeness centrality were calculated for 8 Key targets, and values are mentioned in Table 5. ALB has the highest degree of 81, betweenness and closeness centrality of 0.128046, and 0.7173913, respectively, and TSHR has the least degree and betweenness centrality values of 7 and 0.002343, respectively. This shows that ALB has the strongest interaction in the network. Through the backbone network, the active compounds of MF may act on inflammation and inflammatory-related diseases.

3.7. Biological Process and Pathway Enrichment Analysis

To understand the therapeutic mechanism of MF anti-inflammatory we analyzed systematically GO biological process and Kegg Pathway analysis for key targets using the ShinyGo database. The results showed that the main biological process referring to targets includes Response to oxygen-containing compound (GO:1901700), Cellular response to hormone stimulus (GO:0032870), Response to hormone (GO:0009725), Cellular response to oxygen-containing compound (GO:1901701), and Regulation in apoptotic process (GO:0043065). The enriched top20 biological process is illustrated in Figure 5a.

The results of Kegg pathway analysis showed 13 enriched pathways [Figure 5b], in which pathways in cancer, thyroid hormone synthesis,

Table 2a: Molecular properties of active phytoconstituents by Molinspiration (https://www.molinspiration.com/).

S. No.	Active compounds	Molecular properties				
		MW	TPSA	nON	nOHNH	nROTB
MF1	(−)-Epicatechin	290.27	110.37	6	5	1
MF4	2,4-Di-tert-butylphenol	206.33	20.23	1	1	2
MF6	Betulinic acid	456.71	57.53	3	2	2

MW: Molecular weight, TPSA: Polar surface area, nON: Number of donors, nOHNH: Number of acceptors, nROTB- Number of rotatable bonds

Table 2b: Biological properties of active phytoconstituents by Molinspiration (https://www.molinspiration.com/).

S. No.	Biological properties					
	GPCR ligand	Ion channel modulator	Kinase inhibitor	Nuclear receptor ligand	Protease inhibitor	Enzyme inhibitor
MF1	0.41	0.14	0.09	0.60	0.26	0.47
MF4	−0.37	0.05	−0.51	−0.07	−0.64	−0.07
MF6	0.31	0.03	−0.50	0.93	0.14	0.55

Table 2c: ADMET properties of active compounds by preADMET (https://preadmet.bmdrc.kr/).

S. No.	HIA (%)	PPB (%)	BBB (%)	Caco2 (nm/s)	Skin-permeability
MF1	100.000000	100.000000	20.9638	47.1744	−2.10144
MF4	100.000000	100.000000	10.0918	44.8684	−0.739126
MF6	66.707957	100.000000	0.394913	0.656962	-4.29301

HIA: Human intestinal absorption, BBB: Blood brain barrier, PPB: Plasma protein binding, Caco2: Cacs2 cell permeability

Table 2d: Biological active prediction of compounds by PAS Sonline tool (http://www.pharmaexpert.ru/passonline/).

Compound	Probablity to be active (Pa)
MF1	0.548
MF4	0.762
MF6	0.741

and cAMP signaling pathways are connected to targets and are closely related to the mechanism of MF.

3.8. Molecular Docking

Using molecular docking, the interaction between key targets and compounds is validated. In docking studies, the RMSD has frequently been used to assess the reproducibility of a known binding position. The grid coordinate values set were listed in Table 6a and docking results of the active compounds, MF1, MF4, and MF6, with AR, ESR1, CYP19A1, RARA, NFE2L2, TSHR, NFKB1, and ALB shown in [Figure 6a-h]. Binding affinity and hydrogen bonds formed are listed in Table 6b.

Compared with standard Diclofenac, MF1 exhibited better docking efficiency with all major proteins, in which RARA has a higher binding affinity of −8.3 kcal/mol and forms 3 hydrogen bonds with Leu202, His195, and Tyr277 of bond length 2.86, 3.18, and 3.18Å respectively, and is the best-docked confirmation. MF6 also has the best docking result with all proteins except ESR1 and TSHR. With ALB, MF6 showed the highest binding affinity −9.2 kcal/mol and formed 2 hydrogen bonds of bond length 2.75Å (Arg257) and 3.28Å (Ser454). However, all the docked molecules showed more hydrophobic interactions. Therefore, the best-docked confirmations, MF1-RARA and MF6-ALB complexes are subjected to MD simulation process. Detailed docking result is mentioned in Supplementary Table 2b1-b7 and Supplementary Figure 1a-h.

3.9. MD Simulation Studies

MD simulation was performed to evaluate the dynamic behavior of native proteins and complexes within a nanosecond (ns) time scale. It helps to understand the response of the biomolecular system over time, including the conformational transition, protein folding, and protein-ligand interaction [26]. Based on docking results, ALB-MF6 and RARA-MF1 complexes are considered for MD simulation.

To elucidate the protein-ligand stability and protein structural flexibility between the docked complex ALB-MF6 and RARA-MF1,

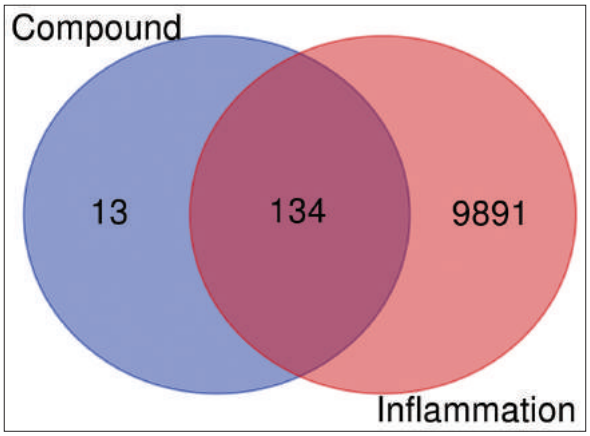

Figure 2: Venn diagram showing the intersection of compound targets and disease targets, intersected part contains targets of both compound and disease i.e., compound-disease target.

we performed 100 ns MD simulation using GROMACS software. The average displacement of the atoms at a simulation instant with a reference structure was calculated by RMSD and RMSF. The RMSD result of ALB stabilized around 22 ns and remained stable up to 75 ns and slight perturbation were observed between 75 and 80 ns and again attains stability up to 100 ns, which validates structural order parameters. The complex structure of ALB-MF6 is constant up to 50 ns and there is perturbation from 50 to 60 ns and finally stable up to 100 [Figure 7a]. In RARA, the RMSD result was observed to be stable till 50 ns and there is a slight variation in the graph from 50 to 60 ns and then up to 100 ns, again attaining stability. The RARA-MF1 complex structure shows constant stability up to 100 ns from the initial point [Figure 7b].

Figure 7c and d show the RMSF plots of Cα atoms in docked complex ALB-MF6 and RARA-MF1, respectively. For ALB protein, slight fluctuations in amino acids Leu430 and Lys500 were observed at RMSF 0.2 nm and 0.45 nm. In the ALB-MF6 complex, there is a slight fluctuation in RMSF (0.35 nm) initially at Lys20 and Glu100residue, then at Leu275 residue (~0.25 nm RMSF) [Figure 7c]. In the case of RARA protein, the fluctuation was observed at 0.25 nm in Tyr178, Cys203, Leu205, Ser219, and Leu405 residues, are shown in Figure 7d.

Solvent accessible surface area (SASA) was assessed to know the protein's conformational stability in the solvent environment. It was found that at 320 nm^2 and 130 nm^2 SASA values, the ALB-MF6

Table 3a: List of compounds' targets from different primary databases and their Uniprot id's (https://www.uniprot.org/).

Gene symbol	Uniprot id	Gene symbol	Uniprot id	Gene symbol	Uniprot id	Gene symbol	Uniprot id
PTH1R	Q03431	ATF6	P18850	ALB	P02768	GLI3	P10071
MAPK10	P53779	CFTR	P13569	HCK	P08631	ESRRG	P62508
CCNA2	P20248	PLAU	P00749	RAPGEF4	Q8WZA2	LMNB1	P20700
SLCO1B1	Q9Y6L6	BMP2	P12643	SP1	P08047	HSP90	P07900
TP53	P04637	TSHR	P16473	CTSL	P07711	NOS3	P29474
HAS2	Q92819	CCL2	P13500	ALPL	P05186	NR1H4	Q96RI1
RACGAP1	Q9H0H5	ABCG2	Q9UNQ0	ACE	P12821	GMNN	O75496
VDR	P11473	BAZ2B	Q9UIF8	AKR1C2	P52895	GLP1R	P43220
RXRA	P19793	NOS1	P29475	PRKCB	P05771	NR1H3	Q13133
PPIA	P62937	PTGS1	P23219	TDP1	Q9NUW8	APOBEC3G	Q9HC16
XDH	P47989	HSD17B10	Q99714	BIRC5	O15392	KDR	P35968
KPNB1	Q14974	CASP7	P55210	GRIN1	Q05586	HMOX1	P09601
CYP2C9	P11712	AKR1B10	O60218	MAPK8	P45983	NQO1	P15559
POLH	O75417	KMT2A	Q03164	GALC	P54803	GAA	P10253
GSK3B	Q9Y253	CES1	P23141	KDM4E	B2RXH2	GPBAR1	Q8TDU6
UBA2	P49841	CYP1A2	P05177	AR	P10275	PTGS2	P35354
POLK	Q9UBT2	ESRRA	P11474	HIF1A	Q16665	PNLIP	P16233
SAE1	Q9UBT6	RAN	P62826	PPARD	Q03181	CHEK1	O14757
POLI	Q9UBE0	IL6	P05231	CYP3A4	P08684	GSR	P00390
CDK2	Q9UNA4	APEX1	P27695	ALPG	P10696	IDH1	O75874
SMAD3	P24941	BACE1	P56817	STS	P08842	CYP2C19	P33261
CREB1	P84022	ESR1	P03372	PRKCE	Q02156	COMT	P21964
TOP1	P16220	NR1I3	Q14994	AKT1	P31749	APOBEC3F	Q8IUX4
TOP2A	P11388	PLA2G7	Q13093	CYP2D6	P10635	TNF	P01375
UBE2I	P63279	BCHE	P06276	NFKB1	P19838	HSPB1	P04792
ALPI	P09923	MAPT	P10636	ALPPL2	P10696	PLAT	P00750
APOA2	P02652	IL1A	P01583	ESR1	P03372	GRIA2	P42262
BCL2	P10415	TTR	P02766	TRAP1	Q12931	PIM1	P11309
RNASE1	P07998	RELA	Q04206	PGR	P06401	NR1H2	P55055
CASP3	P42574	CYP19A1	P11511	F2	P00734	GLI1	P08151
DPP4	P27487	MET	P08581	CRTC2	Q53ET0	IL2	P60568
NCOA2	Q15596	NR3C1	P04150	PGD	P52209	NOS2	P35228
AKR1B1	P15121	RGS4	P49798	DUOX2	Q9NRD8	GCLC	P48506
MEN1	O00255	SNUPN	O95149	NFE2L2	Q16236	FASN	P49327
JUN	P05412	RARA	P10276	POLB	P06746	DHFR	P00374
GSS	P48637	THRB	P10828	CYCS	P99999	SLCO1B3	Q9NPD5
IFNG	P01579	CA2	P00918				

TSHR: Thyrotropin receptor, RARA: Retinoic acid receptor alpha, ALB: Albumin, NFKB1: Nuclear factor kappa B subunit 1, ESR1: Estrogen receptor alpha

[Figure 7e] and RARA-MF1 complexes [Figure 7f] respectively show constant stable conformational dynamics. The conformational stability of complexes can also be evaluated by the Radius of gyration (Rg's) time evolution plot. The ALB Rg stabilizes from 20 ns to 70 ns, then increases at ~72 ns (1.84 nm Rg) and reaches stability up to 100 ns. In complex structures, a slight increase in the plot can be detected at 80 ns [Figure 7g]. Hence, there is no such variation observed in the case of both native protein ALB and complex. The radius of gyration (Rg) of the RARA complex protein (1.86 nm) remained relatively stable, with minimal perturbations observed during the time interval of 50 to 60 nanoseconds [Figure 7h].

The protein system hydrogen bonding pattern also determined the steady trend. The plot shows that during the 100ns period of simulation times, the hydrogen bond in the complex of ALB-MF6 and RARA-MF1 exhibits consistent trends shown in Figure 7i and j.

3.10. Free Binding Energy Calculation

The MM-GBSA calculations were carried out for in-depth analysis of ALB-MF6 and RARA-MF1 complexes MD data. The estimated binding energy ΔGBinding along with its contributing terms are

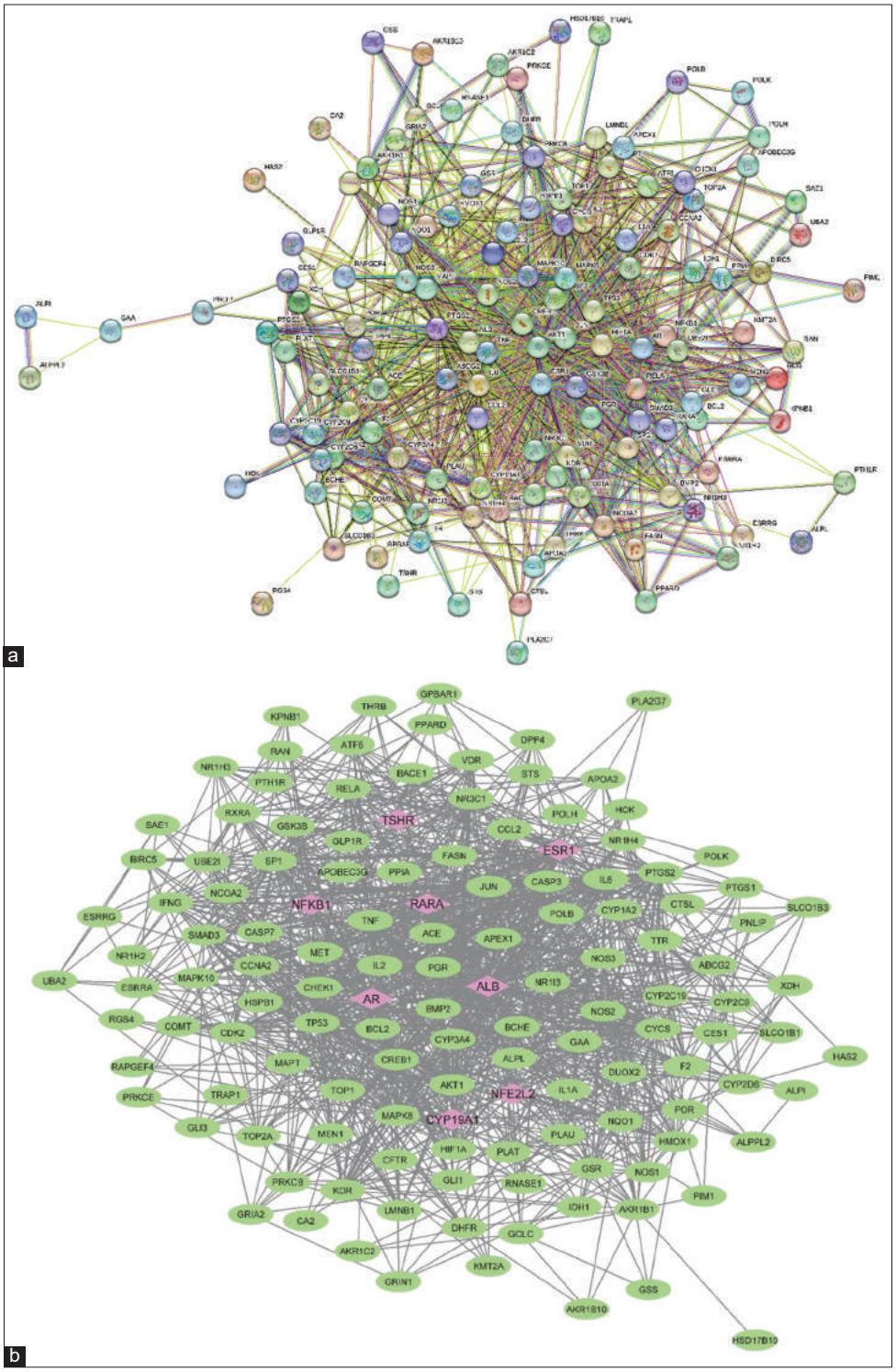

Figure 3: PPI network of compound-disease targets by STRING database (a); (b) shows core interactome network containing major (Hub) proteins, colored in pink with diamond shape.

tabulated in Table 7. The binding energy of −92.29 ± 17.60 KJ/mol and −41.42 ± 14.70 KJ/mol, respectively, was observed for MF6 and MF1 bound to ALB and RARA target complex by using MM-GBSA calculations. Each molecule's relative binding energy is described through energy calculation analysis and gives more reliable results.

4. DISCUSSION

Although inflammation is a necessary component of the body's defensive system and is crucial to the healing process, an overactive inflammatory response can result in a variety of illnesses and disorders. Inflammation is directly linked to chronic diseases,

Table 3b: List of targets involved in both Compound-Target network and Inflammation targets.

CCNA2	PRKCB	ESRRG	HSD17B10	SLCO1B3	CFTR	IDH1	AKR1B1
TP53	GRIN1	KDR	CASP7	PLAT	CCL2	GAA	JUN
HAS2	BIRC5	NR1H4	CYP1A2	CYP2C19	ABCG2	NR1H2	ATF6
XDH	MAPK8	APOBEC3G	CES1	HMOX1	TSHR	GLI1	CA2
VDR	GALC	PTH1R	ESRRA	NQO1	PTGS1	TNF	DHFR
RXRA	HIF1A	MAPK10	RAN	IL2	GPBAR1	BCHE	AR
CYP2C9	CYP3A4	SLCO1B1	APEX1	COMT	GLI3	MAPT	SP1
KPNB1	ALPG	PPIA	BACE1	PTGS2	NOS3	IL1A	ALPL
CDK2	AKT1	POLH	ESR1	PNLIP	CHEK1	TTR	ACE
SMAD3	PRKCE	GSK3B	NR1I3	NOS2	NR1H3	MET	ALPI
CASP3	CYP2D6	UBA2	PLA2G7	HSPB1	CYP19A1	PPARD	APOA2
DPP4	TRAP1	POLK	RELA	LMNB1	RARA	STS	BCL2
NCOA2	PGR	SAE1	NR3C1	POR	HCK	NFKB1	AKR1B10
MEN1	F2	CREB1	RGS4	GLP1R	RAPGEF4	DUOX2	KMT2A
GSS	CYCS	TOP1	ALB	NFE2L2	AKR1C2	GRIA2	IL6
BMP2	GCLC	TOP2A	THRB	POLB	RNASE1	PIM1	
NOS1	FASN	UBE2I	CTSL	IFNG	PLAU	GSR	

TSHR: Thyrotropin receptor, RARA: Retinoic acid receptor alpha, ALB: Albumin, NFKB1: Nuclear factor kappa B subunit 1, ESR1: Estrogen receptor alpha

Table 4: Comparative topological analysis of core-inteactome and backbone network (https://cytoscape.org/).

Network parameters	Core interactome	Backbone network
Clustering coefficient	0.536	0.446
Number of nodes	133	8
Network density	0.143	0.393
Network centralization	0.478	0.429
Network heterogeneity	0.845	0.538
Shortest paths (%)	17556 (100)	42 (75)
Characteristic path length	2.063	1.524
Average number of neighbors	18.827	2.75
Analysis time (s)	0.084	0.016

Table 5: Topological parameters of major proteins.

S. No.	Name	Degree	Betweenness centrality	Closeness centrality
1.	ALB	81	0.128046	0.7173913
2.	ESR1	55	0.039015	0.62857143
3.	AR	41	0.028069	0.5814978
7.	NFKB1	27	0.003807	0.53658537
6.	NFE2L2	26	0.006107	0.54545455
4.	CYP19A1	21	0.003764	0.53012048
5.	RARA	15	0.001583	0.48888889
8	TSHR	7	0.002343	0.43278689

TSHR: Thyrotropin receptor, RARA: Retinoic acid receptor alpha, ALB: Albumin, NFKB1: Nuclear factor kappa B subunit 1, ESR1: Estrogen receptor alpha

Table 6a: Docking coordinate values of grid center and grid box size.

Proteins	Coordinates	Center	Size
ALB	X	32.355	38
	Y	13.348	38
	Z	9.299	38
ESR1	X	107.929	38
	Y	16.786	38
	Z	97.135	38
AR	X	28.536	30
	Y	2.621	30
	Z	4.235	30
NFKB1	X	34.27	38
	Y	22.736	38
	Z	32.209	38
NFE2L2	X	-6.93	30
	Y	7.862	30
	Z	17.931	30
CYP19A1	X	84.635	22
	Y	52.006	22
	Z	57.207	22
RARA	X	31.044	36
	Y	50.692	36
	Z	19.449	36
TSHR	X	2.189	32
	Y	90.626	32
	Z	9.448	32

TSHR: Thyrotropin receptor, RARA: Retinoic acid receptor alpha, ALB: Albumin, NFKB1: Nuclear factor kappa B subunit 1, ESR1: Estrogen receptor alpha

including asthma, cancer, and other conditions, according to a recent study [27]. Inflammation is not only a local response but also a hormone-controlled process. Humans have used herbal remedies as an alternative to treat many diseases for a very long time when there were no effective treatments available. The anti-inflammatory therapeutic efficacy of the medicinal plant is extensively used in the Indian system of medicine. Several studies have conducted anti-inflammatory effects

on MF stem bark, and it has been demonstrated that it has significant anti-inflammatory effects on cell and animal models [11,12]. However, the detailed and systematic molecular mechanism by which MF stem bark inhibits inflammation remains uncertain. Network pharmacology aims to explore the relationship between drugs and diseases based on multi-target analysis. The novel targets and the unknown signaling pathways associated with compounds can be easily determined using network pharmacology. Therefore, the present study is aimed at systematically investigating the potential protein targets and signaling pathways of MF stem bark phytoconstituents using the network pharmacology approach. To verify the results of network pharmacology, docking studies and MD simulations were performed.

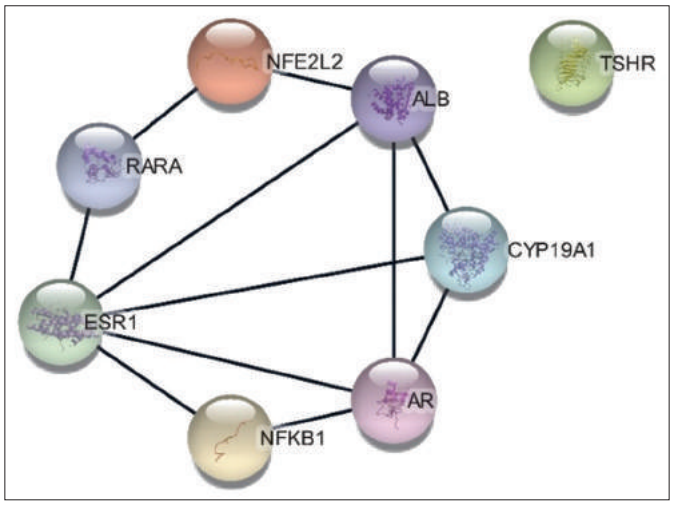

Figure 4: Backbone network from core-interactome network.

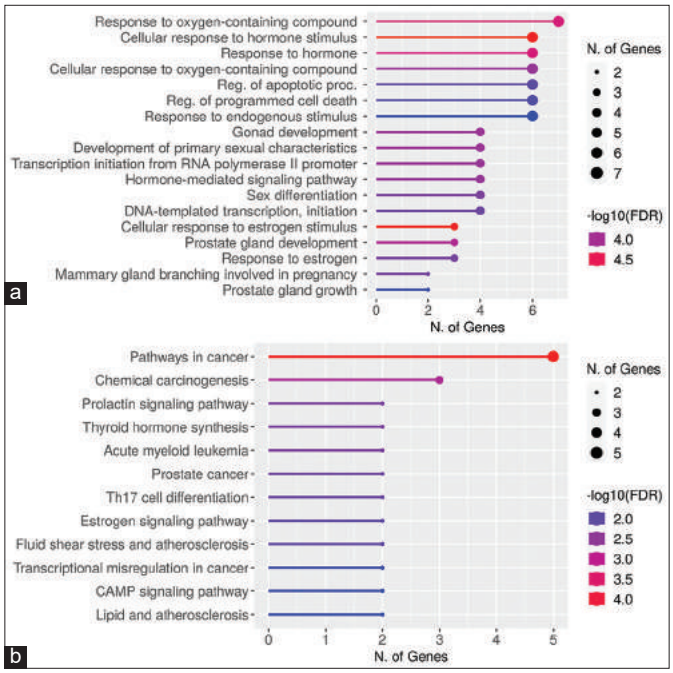

Figure 5: (a) Gene ontology enriched biological process based on the number of genes involved, where the size of the lollipop bubble corresponds to the number of genes and color based on FDR value. (b) Top 13 enriched Kegg Pathway by ShinyGo, size of the lollipop bubble corresponds to the number of genes and color based on FDR value.

In the present work, we explored the bioactive present in MF stem bark by employing HR-LCMS and conducting a literature survey. By comparing the results of both, common bioactive compounds were screened-out to investigate potential targets and their mechanism of action by network pharmacology. The establishment of a "compound-protein/disease-gene" network using network pharmacology is an integrated *in-silico* method for elucidating the processes underlying the synergistic therapeutic effects of conventional drugs [28].

The active compounds structural information is obtained from chemical databases such as PubChem and Chembl, which reveal the structural activity relationship of the compounds. For a molecule to be a drug, 2D structure-based toxicity prediction is the foremost criterion and it serves as the first step toward evaluating its toxicity in *in-vivo*. Hence, the drug-likeness of the compound is evaluated using a free online server preADMET. PIN construction and analysis of targets lead to the understanding of the interaction between the targets. Here we considered AR, ESR1, CYP19A1, RARA, NFE2L2, TSHR, NFKB1, and ALB as major proteins because they are common in active compounds. The network constructed from these proteins acts as the backbone network for the PIN and topological parameters are analyzed for the proteins to know the gene pattern in the interaction network.

ALB and inflammation have a complicated bidirectional relationship and it appears that depending on the pathophysiological situation, serum ALB may either stimulate or moderate immune activation [29]. Reported that by regulating MAPK/NF-kB signaling pathway, ALB inhibits lung inflammation in asthmatic mice [30]. ALB plays a vital role in vascular endothelium's homeostasis by protecting against inflammation. By binding to pro-inflammatory cytokines and reactive oxygen species, ALB moderates the effect of inflammation indirectly [31,32].

Many studies have shown that NFE2L2/NRF2 plays a vital role in inflammation and negative regulation in the NF-kB signaling pathway. It reduces inflammation by inhibiting pro-inflammatory cytokine gene transcription directly or by reducing the activity of NF-kB signaling [33,34]. NRF2 prevents tissue and cell damage by reducing oxidative stress and reducing the production of danger-associated molecular patterns, which are generated by necrotic cells and inflammatory responses. As a master regulator for redox homeostasis, NRF2 indirectly regulates NF-kB activity and also induces anti-inflammatory phenotype, which modulates $CD8^+$ T cells and macrophage function. Pharmaceutical amplification of NRF2 prevents acute inflammatory liver injury in T-cell mediated model of acute inflammatory liver injury [35-37].

Sorisky and Gagnon reported that TSHR may be involved in triggering inflammation and insulin resistance in adipose tissue [38]. The activity of TSHR stimulating immunoglobulins expressed by pretibial fibroblasts on TSHR will provoke the release of cytokines and antigen-specific T-cell responses, leading to systematic inflammation [39]. Reported that the transcription factor NFKB1, a major cellular regulator of inflammation and immunity, was substantially elevated in macrophages [40]. Saccani *et al*. showed that the pro-inflammatory phenotype of tumor-

Table 6b: Docking result with binding affinity and H-bonds formed.

Ligands/Proteins	ALB (1H9Z)		ESR1 (1A52)		AR (2AMA)		NFKB1 (1SVC)		NFE2L2 (3ZGC)		CYP19A1 (3EQM)		RARA (3A9E)		TSHR (3G04)	
	Affinity (kcal/mol	H-bonds	Affinity (kcal/mol	H-bonds	Affinity (kcal/mol	H-bonds	Affinity (kcal/mol	H-bonds	Affinity (kcal/mol	H-bonds	Affinity (kcal/mol	H-bonds	Affinity (kcal/mol	H-bonds	Affinity (kcal/mol	H-bonds
MF1	−7.8	3	−7.9	1	−7.2	2	−6.3	2	−7.4	4	−8.1	2	−8.3	3	−6.9	4
MF4	−6.4	1	−7.1	1	−6.0	2	−4.9	2	−6.5	1	−5.2	2	−7.6	1	−5.2	2
MF6	−9.2	2	−7.0	1	−6.9	4	−6.6	4	−7.0	2	−7.0	3	−6.9	3	−5.7	2
DICLOFENAC	−7.7	1	−8.4	1	−7.6	1	−5.6	1	−6.5	2	−5.7	2	−7.3	1	−5.7	2

TSHR: Thyrotropin receptor, RARA: Retinoic acid receptor alpha, ALB: Albumin, NFKB1: Nuclear factor kappa B subunit 1, ESR1: Estrogen receptor alpha.

Table 7: Binding energy and the contribution energy terms of ALB-MF6 and RARA-MF1 complexes calculated using MM-GBSA module.

Type of energy	Energy contributed (KJ/mol)	
	ALB-MF6 complex	RARA-MF1 complex
Van der Waal energy	−188.99±17.20	−127.53±14.31
Electrostatic energy	−20.60±6.85	−24.81±7.78
Polar solvation energy	139.88±25.86	124.84±23.62
SASA energy	−22.58±1.31	−13.92±1.24
Binding energy	−92.29±17.60	−41.42±14.70

RARA: Retinoic acid receptor alpha, ALB: Albumin, SASA: Solvent accessible surface area, MM-GBSA: Molecular mechanics and generalized born surface area

associated macrophages is inhibited by NFkB [41]. It has been demonstrated that NFkB homodimers, which lack transactivation domains, suppress the expression of NFkB target genes and reduce inflammation. According to some studies, NFkB can directly inhibit the expression of proinflammatory genes and regulate the expression or activity of anti-inflammatory cytokines like IL-10 to reduce inflammation [42].

AR in macrophages promotes inflammation and blocks the healing of wounds by upregulating the expression of TNFα. Monocytes/macrophages have been found to express AR, indicating that AR may affect the actions of macrophages in these inflammatory conditions [43,44]. Mohammad *et al*., have reported that ESR1 in T cells plays a significant role in inflammation and ESR1-targeted immunotherapies may effectively treat autoimmune diseases [45]. RARA has been found to have immunosuppressive effects in cardiac transplantation by preventing cytotoxic T-cells and alloantigen-stimulated generation of pro-inflammatory cytokines, demonstrating how RARA selective agonists and antagonists affect inflammatory processes [46]. Based on these studies, the major proteins can play a role as anti-inflammatory targets and could be used as therapeutic targets.

We performed GO biological process enrichment and pathway enrichment analysis using the ShinyGo server. We considered the top 20 enriched GO terms and pathways based on the number of genes involved, wherein "Response to the oxygen-containing compound" was the enriched GO biological process. Out of the top 13 enriched pathways, Pathways in cancer, Thyroid hormone synthesis, and cAMP signaling pathways have robust connections with inflammation. The majority of cancers are affected by inflammation, but inflammation is also impacted by cancer; therefore, the relationship between inflammation and cancer is two-edged. Cancer-related inflammation is the key characteristic of cancer, which is caused by cancer-initiating mutations and leads to tumor progression through the activation of inflammatory cells and also promotes immunosuppression of tumor microenvironment [47-49]. Recent studies have shown a direct link between thyroid hormones and inflammation by controlling the transcription of genes implicated in inflammatory-related pathways. Thyroid hormones act as inflammatory modulators through their nuclear receptors [50]. Activation of the cAMP signaling pathway through inflammatory mediators can limit the tissue injury process and is a pharmacological approach to treating inflammatory diseases and controlling the resolution of inflammation [51,52]. As cAMP signaling is dependent on PKA, by inhibiting PKA can treat inflammation in immune responses through cAMP signaling pathway [53].

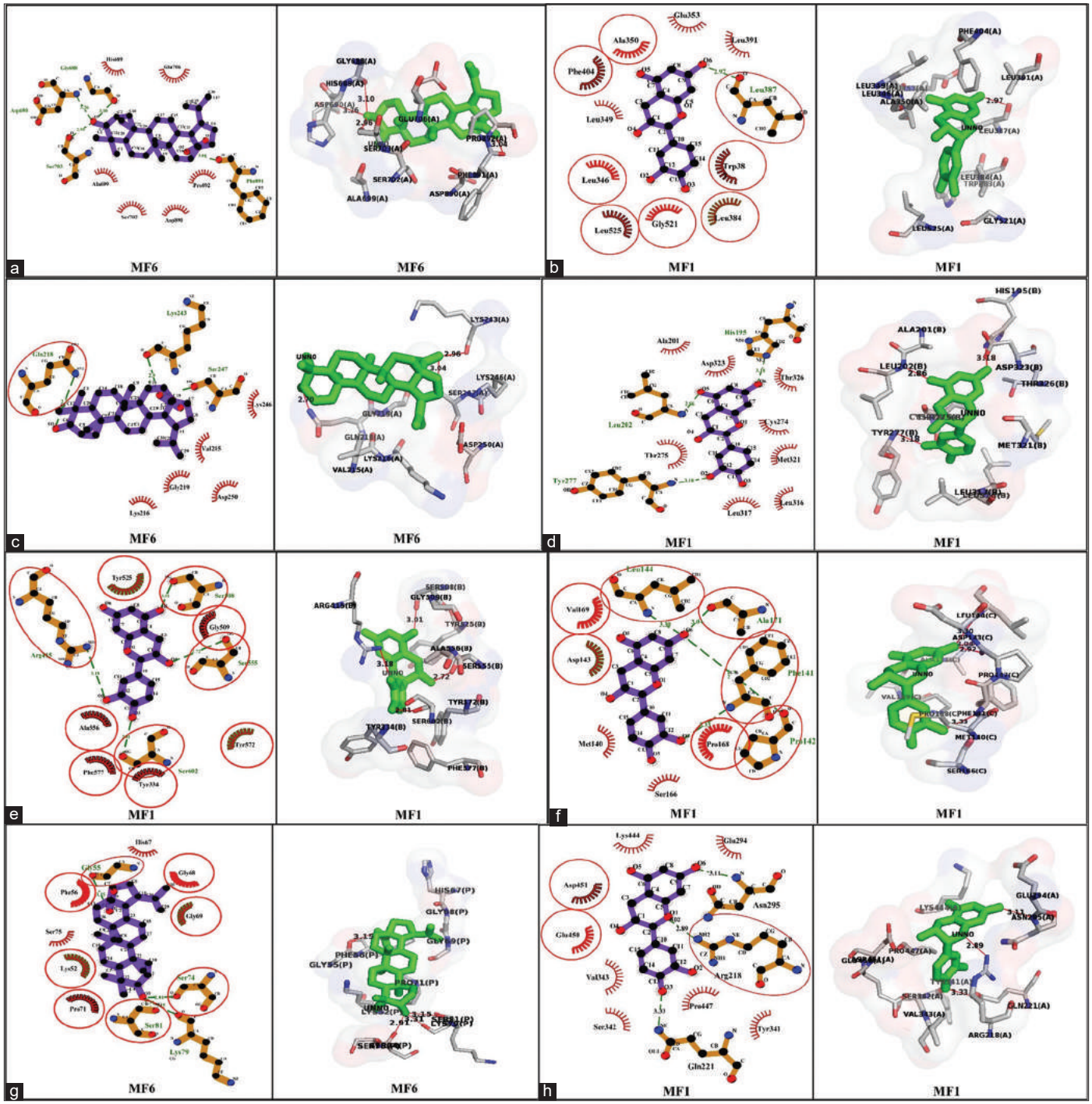

Figure 6: 2D and 3D results of best-docked poses (a) MF6-AR, (b) MF1-ESR1, (c) MF6-CYP19A1, (d) MF1-RARA, (e) MF1-NFE2L2, (f) MF1-TSHR, (g) MF1-NFKB1, (h) MF1-ALB, where the compounds are represented in green color and hydrogen bonds with red color.

To know the effective activity of MF phytoconstituents against major targets, docking studies, and MDs simulation were used. Molecular docking was used to predict the binding pattern between the drug and the target. The binding affinity or binding free energy obtained after docking is the interaction score between them. In our results, MF1 and MF6 show better interaction and have a very good binding affinity with all proteins compared to standard Diclofenac. Overall, the docking results show that the major constituents have good efficacy with major proteins. MD simulation analysis was carried out to validate the protein-ligand complex of the docked compound and to measure the stability of the ligand binding in the active site of the selected target. From MM-GBSA analysis of compounds MF1 and MF6 showed significant binding with selected targets RARA and ALB, respectively.

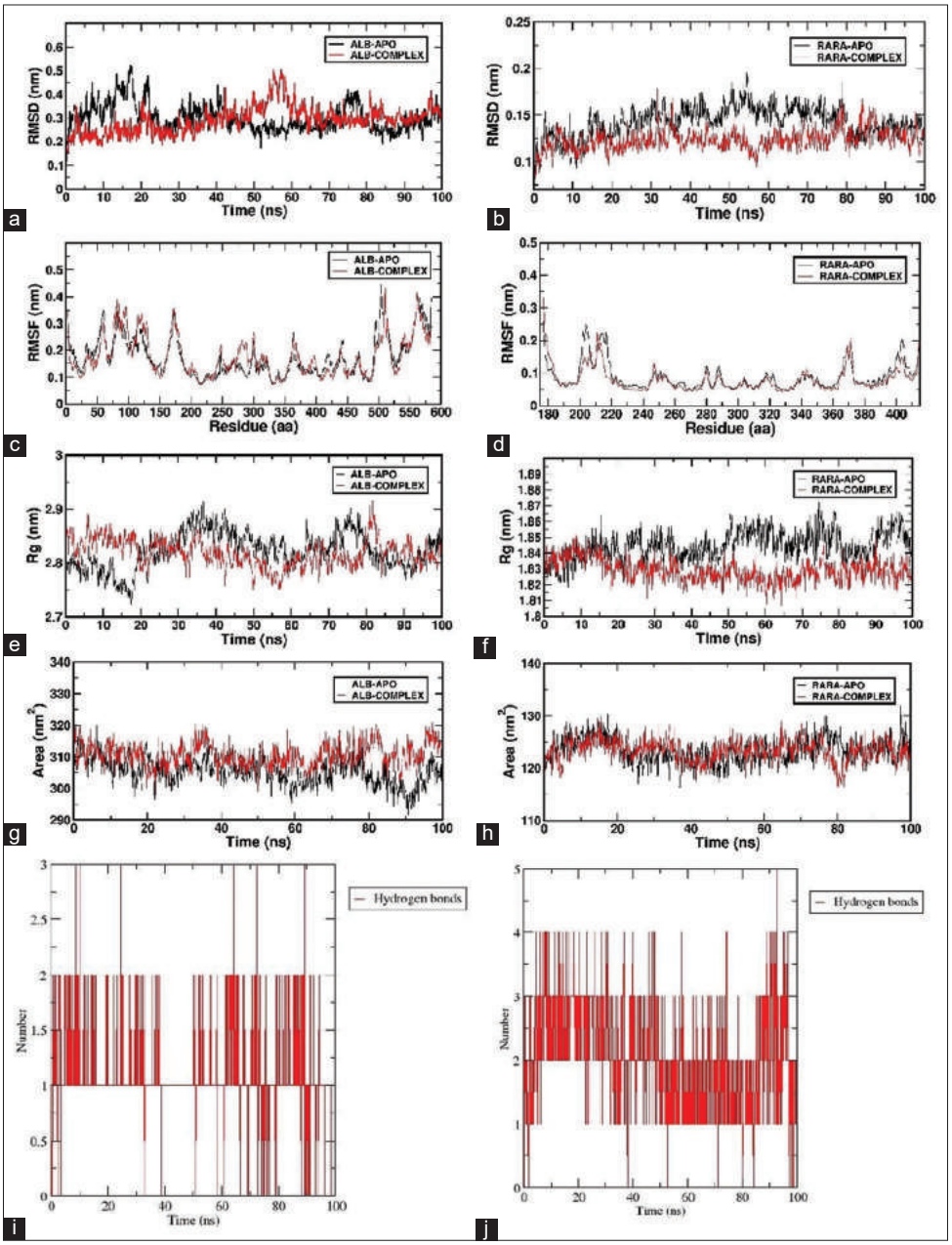

Figure 7: MD simulation results of native proteins (ALB and RARA) and complexes (ALB-MF6 and RARA-MF1). (a and b) represent the RMSD values (y-axis in nanometer) of the protein-ligand complex over simulation time (x-axis in nanosecond), (c and d) show the RMSF values of Cα of native protein and complexes (x-axis represents atoms in protein structure and y-axis represents RMSF values in nanometer), (e and f) represent Rg of unbound ALB and RARA, and bound ALB-MF6 and RARA-MF1 complexes were analyzed. The calculated SASA for all the initial structures of ALB-MF6 and RARA-MF1 complexes are shown in the (g and h), which display a small change in conformation of structures that occurred during the simulation period. Hydrogen-bonding analysis, for the period of simulation time under consideration the formation of hydrogen bonds for stabilizing the structure of ALB-MF6 and RARA-MF1 was observed in (i and j) respectively.

5. CONCLUSION

This study establishes a scientific foundation for determining the efficacy of multicomponent, multi-target drug treatment as well as finding novel anti-inflammatory therapeutic targets. In this study, network pharmacology, molecular docking, and MD simulation were employed to explore the underlying mechanism against inflammation. Through network analysis, it was found that MF contains multi-targeting compounds that function on numerous disease-related pathways; hence, it may be considered that MF plays an important role in treating inflammation. Furthermore, our studies revealed that (-)-epicatechin, 2,4-di-tert-butylphenol, and betulinic acid play a critical role in inflammation by docking with AR, ESR1, CYP19A1, RARA, NFE2L2, TSHR, NFKB1 and ALB genes, which provides an important basis for further investigations. However, *in-vitro* studies are needed to further validate our findings.

6. ACKNOWLEDGMENT

The authors thank the Directorate of Minorities, Government of Karnataka, for providing financial support through the minority fellowship program and the Kuvempu University administrative authority for offering the facility to carry out the work.

7. AUTHORS' CONTRIBUTIONS

All authors made substantial contributions to the conception and design, acquisition of data, or analysis and interpretation of data; took part in drafting the article or revising it critically for important intellectual content; agreed to submit to the current journal; gave final approval of the version to be published; and agreed to be accountable for all aspects of the work. All the authors are eligible to be an author as per the International Committee of Medical Journal Editors (ICMJE) requirements/guidelines.

8. CONFLICT OF INTEREST

The authors report no financial or any other conflicts of interest in this work.

9. ETHICAL APPROVALS

This study does not involve experiments on animals or human subjects.

10. DATA AVAILABILITY

All data generated in this paper is available in the body of the manuscript as tables and figures, and also in the supplementary tables and figure.

11. PUBLISHER'S NOTE

This journal remains neutral with regard to jurisdictional claims in published institutional affiliation.

REFERENCES

1. Vodovotz Y, Constantine G, Rubin J, Csete M, Voit EO, An G. Mechanistic simulations of inflammation: Current state and future prospects. Math Biosci 2009;217:1-10.
2. Noor F, Qamar MT, Ashfaq UA, Albutti A, Alwashmi AS, Aljasir MA. Network pharmacology approach for medicinal plants: Review and assessment. Pharmaceuticals 2022;15:572.
3. Dong Y, Zhao Q, Wang Y. Network pharmacology-based investigation of potential targets of astragalus membranaceous-angelica sinensis compound acting on diabetic nephropathy. Sci Rep 2021;111:19496.
4. Saeidnia S, Manayi A, Abdollahi M. The pros and cons of the *in-silico* pharmaco-toxicology in drug discovery and development. Int J Pharmacol 2013;9:176-81.
5. Rahman SM, Shabnom S, Quader MA, Hossain MA. Phytochemical study on the ethylacetate extract of the leaves of *Mesua ferrea* Linn. Indones J Chem 2010;8:242-4.
6. Asif M, Jafari SF, Iqbal Z, Revadigar V, Oon CE, Majid AS, *et al*. Ethnobotanical and Phytopharmacological attributes of *Mesua ferrea*: A mini review. J Appl Pharm Sci 2017;7:242-51.
7. Keawsa-Ard S, Liawruangrath B, Kongtaweelert S. Bioactive compounds from *Mesua ferrea* stems. Chiang Mai J Sci 2015;42: 186-96.
8. Chahar MK, Kumar DS, Lokesh T, Manohara KP. *In-vivo* antioxidant and immunomodulatory activity of mesuol isolated from *Mesua ferrea* L. seed oil. Int Immunopharmacol 2012;13:386-91.
9. Chanda S, Rakholiya K, Parekh J. Indian medicinal herb: Antimicrobial efficacy of *Mesua ferrea* L. seed extracted in different solvents against infection causing pathogenic strains. J Acute Dis 2013;2:277-81.
10. Mazumder R, Dastidar SG, Basu SP, Mazumder A, Singh SK. Antibacterial potentiality of *Mesua ferrea* Linn. flowers. Phyther Res 2004;18:824-6.
11. Prathima R, Manjunatha H, Krishna V, Kandagalla S, Sharath BS. Studies on anti-inflammatory effect of *Mesua ferrea* Linn. in acute and chronic inflammation of experimental animals. Int J Pharm Sci Res 2018;9:517-25.
12. Asif M, Shafaei A, Majid AS, Ezzat MO, Dahham SS, Ahamed MB, *et al*. *Mesua ferrea* stem bark extract induces apoptosis and inhibits metastasis in human colorectal carcinoma HCT 116 cells, through modulation of multiple cell signalling pathways. Chin J Nat Med 2017;15:505-14.
13. Chaithanya KK, Gopalakrishnan VK, Hagos Z, Nagaraju B, Kamalakararao K, Kebede H, *et al*. *In vitro* and *in vivo* anti-inflammatory activities of *Mesua ferrea* Linn. Int J Pharmacogn Phytochem Res 2018;10:103-11.
14. Singh S, Gray AI, Waterman PG. Mesuabixanthone-A and mesuabixanthone-B: Novel bis-xanthones from the stem bark of *Mesua ferrea* (Guttiferae). Nat Prod Lett 2006;3:53-8.
15. Islam R, Ahmed I, Sikder AA, Haque MR, Al-Mansur A, Ahmed M, *et al*. Chemical investigation of *Mesua nagassarium* (Burm. f.) kosterm. J Basic Appl Sci 2014;10:124-8.
16. Gaulton A, Hersey A, Nowotka ML, Bento AP, Chambers J, Mendez D, *et al*. The ChEMBL database in 2017. Nucleic Acids Res 2017;45:D945-54.
17. Filimonov DA, Lagunin AA, Gloriozova TA, Rudik AV, Druzhilovskii DS, Pogodin PV, *et al*. Prediction of the biological activity spectra of organic compounds using the pass online web resource. Chem Heterocycl Compd 2014;50:444-57.
18. Shannon P, Markiel A, Ozier O, Baliga NS, Wang JT, Ramage D, *et al*. Cytoscape: A software environment for integrated models of biomolecular interaction networks. Genome Res 2003;13:2498-504.
19. Franceschini A, Szklarczyk D, Frankild S, Kuhn M, Simonovic M, Roth A, *et al*. STRING v9.1: Protein-protein interaction networks, with increased coverage and integration. Nucleic Acids Res 2013;41:D808-15.
20. Assenov Y, Ramírez F, Schelhorn SE, Lengauer T, Albrecht M. Computing topological parameters of biological networks. Bioinformatics 2008;24:282-4.
21. Ge SX, Jung D, Yao R. ShinyGO: A graphical gene-set enrichment tool for animals and plants. Bioinformatics 2020;36:2628-9.
22. Trott O, Olson AJ. AutoDock Vina: Improving the speed and accuracy of docking with a new scoring function, efficient optimization, and multithreading. J Comput Chem 2010;31:455-61.
23. Laskowski RA, Swindells MB. LigPlot+: Multiple ligand-protein interaction diagrams for drug discovery. J Chem Inf Model 2011;51:2778-86.
24. Hess B, Bekker H, Berendsen HJ, Fraaije JG. LINCS: A linear constraint solver for molecular simulations. J Comput Chem 1997;18:1463-72.
25. Jin Z, Wang Y, Yu XF, Tan QQ, Liang SS, Li T, *et al*. Structure-based virtual screening of influenza virus RNA polymerase inhibitors from natural compounds: Molecular dynamics simulation and MM-GBSA calculation. Comput Biol Chem 2020;85:107241.
26. Karplus M, McCammon JA. Molecular dynamics simulations of biomolecules. Nat Struct Biol 2002;9:646-52.
27. Hedin U, Matic LP. Recent advances in therapeutic targeting of inflammation in atherosclerosis. J Vasc Surg 2019;69:944-51.
28. Zhang R, Zhu X, Bai H, Ning K. Network pharmacology databases for traditional Chinese medicine: review and assessment. Front

Pharmacol 2019;10:123.
29. Dirajlal-Fargo S, Kulkarni M, Bowman E, Shan L, Sattar A, Funderburg N, *et al*. Serum albumin is associated with higher inflammation and carotid atherosclerosis in treated human immunodeficiency virus infection. Open Forum Infect Dis 2018;5:ofy291.
30. Cai Z, Liu J, Bian H, Cai J. Albiflorin alleviates ovalbumin (OVA)-induced pulmonary inflammation in asthmatic mice. Am J Transl Res 2019;11:7300-9.
31. Van Ancum JM, Tuttle CS, Koopman R, Pijnappels M, Meskers CG, Paul SK, *et al*. Albumin and C-reactive protein relate to functional and body composition parameters in patients admitted to geriatric rehabilitation after acute hospitalization: Findings from the RESORT cohort. Eur Geriatr Med 2022;13:623-32.
32. Artigas A, Wernerman J, Arroyo V, Vincent JL, Levy M. Role of albumin in diseases associated with severe systemic inflammation: Pathophysiologic and clinical evidence in sepsis and in decompensated cirrhosis. J Crit Care 2016;33:62-70.
33. Ahmed SM, Luo L, Namani A, Wang XJ, Tang X. Nrf2 signaling pathway: Pivotal roles in inflammation. Biochim Biophys Acta Mol Basis Dis 2017;1863:585-97.
34. He F, Ru X, Wen T. NRF2, a transcription factor for stress response and beyond. Int J Mol Sci 2020;21:4777.
35. Cuadrado A, Manda G, Hassan A, Alcaraz MJ, Barbas C, Daiber A, *et al*. Transcription factor NRF2 as a therapeutic target for chronic diseases: A systems medicine approach. Pharmacol Rev 2018;70:348-83.
36. Sha LK, Sha W, Kuchler L, Daiber A, Giegerich AK, Weigert A, *et al*. Loss of Nrf2 in bone marrow-derived macrophages impairs antigen-driven CD8(+) T cell function by limiting GSH and CYS availability. Free Radic Biol Med 2015;83:77-88.
37. Osburn WO, Yates MS, Dolan PD, Chen S, Liby KT, Sporn MB, *et al*. Genetic or pharmacologic amplification of nrf2 signaling inhibits acute inflammatory liver injury in mice. Toxicol Sci 2008;104:218-27.
38. Sorisky A, Gagnon A. Freedom of expression beyond the thyroid: The thyroid-stimulating hormone receptor in the adipocyte. OA Biochemistry 2014;2:2.
39. Diana T, Kahaly GJ. Thyroid stimulating hormone receptor antibodies in thyroid eye disease-methodology and clinical applications. Ophthalmic Plast Reconstr Surg 2018;34:S13-9.
40. Somma D, Kok FO, Kerrigan D, Wells CA, Carmody RJ. Defining the role of nuclear factor (NF)-κB p105 subunit in human macrophage by transcriptomic analysis of NFKB1 knockout THP1 cells. Front Immunol 2021;12:669906.
41. Saccani A, Schioppa T, Porta C, Biswas SK, Nebuloni M, Vago L, *et al*. p50 nuclear factor-κB overexpression in tumor-associated macrophages inhibits M1 inflammatory responses and antitumor resistance. Cancer Res 2006;66:11432-40.
42. Bohuslav J, Kravchenko VV, Parry GC, Erlich JH, Gerondakis S, Mackman N, *et al*. Regulation of an essential innate immune response by the p50 subunit of NF-kappaB. J Clin Invest 1998;102:1645-52.
43. Lai JJ, Chang P, Lai KP, Chen L, Chang C. The role of androgen and androgen receptor in skin-related disorders. Arch Dermatol Res 2012;304:499-510.
44. Lai JJ, Lai KP, Zeng W, Chuang KH, Altuwaijri S, Chang C. Androgen receptor influences on body defense system via modulation of innate and adaptive immune systems: Lessons from conditional AR knockout mice. Am J Pathol 2012;181:1504-12.
45. Mohammad I, Starskaia I, Nagy T, Guo J, Yatkin E, Väänänen K, *et al*. Estrogen receptor α contributes to T cell-mediated autoimmune inflammation by promoting T cell activation and proliferation. Sci Signal 2018;11:eaap9415.
46. Zisakis A, Katsetos CD, Vasiliou AD, Karachalios T, Li S. Expression of retinoic acid receptor (RAR) α protein in the synovial membrane from patients with osteoarthritis and rheumatoid arthritis. Int J Biomed Sci 2007;3:46-9.
47. Ma Y, Adjemian S, Mattarollo SR, Yamazaki T, Aymeric L, Yang H, *et al*. Anticancer chemotherapy-induced intratumoral recruitment and differentiation of antigen-presenting cells. Immunity 2013;38:729-41.
48. Punt S, Dronkers EA, Welters MJ, Goedemans R, Koljenović S, Bloemena E, *et al*. A beneficial tumor microenvironment in oropharyngeal squamous cell carcinoma is characterized by a high T cell and low IL-17(+) cell frequency. Cancer Immunol Immunother 2016;65:393-403.
49. Zhao H, Wu L, Yan G, Chen Y, Zhou M, Wu Y, *et al*. Inflammation and tumor progression: Signaling pathways and targeted intervention. Signal Transduct Target Ther 2021;6:263.
50. De Castro AL, Fernandes RO, Ortiz VD, Campos C, Bonetto JH, Fernandes TR, *et al*. Thyroid hormones decrease the proinflammatory TLR4/NF-κβ pathway and improve functional parameters of the left ventricle of infarcted rats. Mol Cell Endocrinol 2018;461:132-42.
51. Aslam M, Ladilov Y. Emerging role of cAMP/AMPK signaling. Cells 2022;11:308.
52. Tavares LP, Negreiros-Lima GL, Lima KM, Silva PM, Pinho V, Teixeira MM, *et al*. Blame the signaling: Role of cAMP for the resolution of inflammation. Pharmacol Res 2020;159:105030.
53. Massimi M, Ragusa F, Cardarelli S, Giorgi M. Targeting cyclic AMP signalling in hepatocellular carcinoma. Cells 2019;8:1511.

How to cite this article:
Sundaram JK, Hanumanthappa M, Kandagalla S, Shekarappa SB, Gollapalli P, Hani U. Evaluating the anti-inflammatory potential of *Mesua ferrea* linn. stem bark through network pharmacology approach. J App Biol Biotech. 2023;11(5):174-197.
DOI: 10.7324/JABB.2023.11521

Supplementary Tables

Table 1: HR-LCMS result of stem bark ethanolic extract.

Compound Label	RT	Mass	Abund	Name	Formula	Hits (DB)
Cpd 1: Valine	1.12	117.0795		Valine	C5 H11 N O2	9
Cpd 2: Dihydrocaffeic acid 3-Oglucuronide	1.159	358.0904		Dihydrocaffeic acid 3-Oglucuronide	C15 H18 O10	3
Cpd 3: 1.316	1.316					
Cpd 4: cis-Resveratrol 3-Oglucuronide	5.184	404.1119		cis-Resveratrol 3-Oglucuronide	C20 H20 O9	9
Cpd 5: Hesperetin 7-Oglucuronide	5.385	476.133	27341	Hesperetin 7-O-glucuronide	C23 H24 O11	3
Cpd 6: Gentisin	6.303	258.0534		Gentisin	C14 H10 O5	10
Cpd 7: Kigelinone	6.689	258.0538	25223	Kigelinone	C14 H10 O5	10
Cpd 8: Lecanoric acid	6.847	318.0748	25652	Lecanoric acid	C16 H14 O7	6
Cpd 9: Cirsimaritin	7.11	314.0799		Cirsimaritin	C17 H14 O6	10
Cpd 10: 7.257	7.257					
Cpd 11: Porric acid A	8.15	302.0799	69531	Porric acid A	C16 H14 O6	10
Cpd 12: Urolithin B	8.417	212.048		Urolithin B	C13 H8 O3	4
Cpd 13: Silandrin	8.676	466.1265	22260	Silandrin	C25 H22 O9	3
Cpd 14: Betulinic acid	8.734	456.69	57865	Betulinic acid	C30 H48 O3	10
Cpd 15: a-L-Arabinofuranosyl-(1->2)-[a-D-mannopyranosyl-(1->6)]-D-mannose	8.873	474.1555		a-L-Arabinofuranosyl-(1->2)-[a-D-mannopyranosyl-(1->6)]-D-mannose	C17 H30 O15	3
Cpd 16: Gentianose	8.994	504.1661		Gentianose	C18 H32 O16	10
Cpd 17: Dihydrodeoxystreptomycin	9.007	567.2895	39724	Dihydrodeoxystreptomycin	C21 H41 N7 O11	2
Cpd 18: a-L-Arabinofuranosyl-(1->2)-[a-D-mannopyranosyl-(1->6)]-D-mannose	9.131	474.1554		a-L-Arabinofuranosyl-(1->2)-[a-D-mannopyranosyl-(1->6)]-D-mannose	C17 H30 O15	3
Cpd 19: Silandrin	9.137	466.1269	24905	Silandrin	C25 H22 O9	3
Cpd 20: Dihydroergocristine	9.255	611.3174	11874	Dihydroergocristine	C35 H41 N5 O5	1
Cpd 21: 9.405	9.405		86380			
Cpd 22: Physagulin F	9.559	544.2707		Physagulin F	C30 H40 O9	1
Cpd 23: 9.741	9.741		92213			
Cpd 24: 9.847	9.847		127518			
Cpd 25: Physagulin F	10.157	544.271	74338	Physagulin F	C30 H40 O9	1
Cpd 26: Liquiritigenin	10.326	256.0744		Liquiritigenin	C15 H12 O4	10
Cpd 27: 10.377	10.377		197245			
Cpd 28: 10.639	10.639		289684			
Cpd 29: 4',5-Dihydroxy-3',5',7,8-tetramethoxyflavone	10.82	374.1009	46412	4',5-Dihydroxy-3',5',7,8-tetramethoxyflavone	C19 H18 O8	9
Cpd 30: BQ 123	10.849	606.2992	65991	BQ 123	C31 H42 N6 O7	2
Cpd 31: 6,8a-Seco-6,8a-deoxy-5-oxoavermectin "2b" aglycone	11.027	572.3371	69454	6,8a-Seco-6,8a-deoxy-5-oxoavermectin "2b" aglycone	C33 H48 O8	1
Cpd 32: 4',5,6-Trimethylscutellarein 7-glucoside	11.07	490.1505	45140	4',5,6-Trimethylscutellarein 7-glucoside	C24 H26 O11	1
Cpd 33: all-trans-hexaprenyldiphosphate	11.132	586.3186	160004	all-trans-hexaprenyl diphosphate	C30 H52 O7 P2	5
Cpd 34: 11.196	11.196		26985			
Cpd 35: Cefpiramide	11.343	612.1275	40771	Cefpiramide	C25 H24 N8 O7 S2	2
Cpd 36: Candletoxin A	11.683	608.2992	102672	Candletoxin A	C35 H44 O9	5
Cpd 37: 6,8a-Seco-6,8a-deoxy-5-oxoavermectin "2b" aglycone	11.725	570.3274	89726	6,8a-Seco-6,8a-deoxy-5-oxoavermectin "2b" aglycone	C33 H48 O8	1
Cpd 38: Fusaroskyrin	11.914	598.1114	30253	Fusaroskyrin	C32 H22 O12	7

(*Contd...*)

Table 1: (*Continued*).

Compound Label	RT	Mass	Abund	Name	Formula	Hits (DB)
Cpd 39: 6,8a-Seco-6,8a-deoxy-5-oxoavermectin "2b" aglycone	12.001	570.3271	72872	6,8a-Seco-6,8a-deoxy-5-oxoavermectin "2b" aglycone	C33 H48 O8	1
Cpd 40: Avermectin B1b aglycone	12.033	570.3222	63059	Avermectin B1b aglycone	C33 H46 O8	1
Cpd 41: Avermectin B1b aglycone	12.266	570.3221	58707	Avermectin B1b aglycone	C33 H46 O8	1
Cpd 42: Fusaroskyrin	12.446	598.1118	163724	Fusaroskyrin	C32 H22 O12	7
Cpd 43: Fusaroskyrin	12.723	598.1115	44228	Fusaroskyrin	C32 H22 O12	7
Cpd 44: (-)-Epicatechin	12.986	290.29	86285	(-)-Epicatechin	C15 H14 O6	10
Cpd 45: Hydrocortisone cypionate	13.207	486.3001	14554	Hydrocortisone cypionate	C29 H42 O6	1
Cpd 46: Vulgarone A	13.257	218.1676		Vulgarone A	C15 H22 O	10
Cpd 47: Icariside E5	13.259	522.2164	30422	Icariside E5	C26 H34 O11	9
Cpd 48: Kanamycin	13.271	484.2398	23348	Kanamycin	C18 H36 N4 O11	4
Cpd 49: 13.368	13.368		42688			
Cpd 50: 4'-Hydroxyanigorootin	13.522	590.1451	66094	4'-Hydroxyanigorootin	C38 H22 O7	2
Cpd 51: Bonafousine	13.591	564.3092	226086	Bonafousine	C35 H40 N4 O3	1
Cpd 52: Cefpiramide	13.833	612.128	55919	Cefpiramide	C25 H24 N8 O7 S2	1
Cpd 53: Bonafousine	13.846	564.3092	44611	Bonafousine	C35 H40 N4 O3	1
Cpd 54: alpha-Santalal	13.937	218.1679		alpha-Santalal	C15 H22 O	10
Cpd 55: 4'-Hydroxyanigorootin	14.161	590.1453		4'-Hydroxyanigorootin	C38 H22 O7	2
Cpd 56: Capsaicin	14.289	305.2001		Capsaicin	C18 H27 N O3	1
Cpd 57: 14.867	14.867		156635			
Cpd 58: 14.953	14.953					
Cpd 59: 6-Hydroxykaempferol 6,7-diglucoside	15.021	626.1429	93703	6-Hydroxykaempferol 6,7-diglucoside	C27 H30 O17	7
Cpd 60: 15.093	15.093					
Cpd 61: Lansiumarin B	15.27	370.1449		Lansiumarin B	C21 H22 O6	10
Cpd 62: 6-Hydroxykaempferol 6,7-diglucoside	15.337	626.1428	82176	6-Hydroxykaempferol 6,7-diglucoside	C27 H30 O17	7
Cpd 63: 2,4-Di-tert-butylphenol	15.342	206.30	41087	2,4-Di-tert-butylphenol	C14 H22 O	10
Cpd 64: Lansiumarin B	15.481	370.1449		Lansiumarin B	C21 H22 O6	10
Cpd 65: Boviquinone 4	15.885	412.2623		Boviquinone 4	C26 H36 O4	10
Cpd 66: 15.885	15.885		117504			
Cpd 67: 23-Acetoxysoladulcidine	15.975	473.3512	58096	23-Acetoxysoladulcidine	C29 H47 N O4	1
Cpd 68: Phytosphingosine	16.214	317.2936		Phytosphingosine	C18 H39 N O3	1
Cpd 69: Cytochalasin Opho	16.287	451.2724		Cytochalasin Opho	C28 H37 N O4	3
Cpd 70: 23-Acetoxysoladulcidine	16.288	473.3514	85473	23-Acetoxysoladulcidine	C29 H47 N O4	1
Cpd 71: 16.385	16.385		51082			
Cpd 72: Ciclesonide	16.457	540.3124	126293	Ciclesonide	C32 H44 O7	1
Cpd 73: Fosinopril	16.614	562.2966	60271	Fosinopril	C30 H46 N O7 P	1
Cpd 74: 16.692	16.692		118439			
Cpd 75: 16.693	16.693		104094			
Cpd 76: 16.896	16.896		48158			
Cpd 77: 16.957	16.957					
Cpd 78: 17.029	17.029					
Cpd 79: 17.172	17.172					
Cpd 80: 17.326	17.326		98981			
Cpd 81: Neomycin B	17.33	614.3167		Neomycin B	C23 H46 N6 O13	2
Cpd 82: A 80987	17.4	653.3251	26992	A 80987	C37 H43 N5 O6	1
Cpd 83: Methyllycaconitine	17.752	682.3403	34643	Methyllycaconitine	C37 H50 N2 O10	1

(*Contd...*)

Table 1: (*Continued*).

Compound Label	RT	Mass	Abund	Name	Formula	Hits (DB)
Cpd 84: Pheophorbide a	17.845	592.2697	26450	Pheophorbide a	C35 H36 N4 O5	2
Cpd 85: (5b,7a,12a)-2-(3-methoxyphenyl)-2-oxoethyl ester-7,12-dihydroxy-cholan-24-oic acid	18.093	540.3441	18665	(5b,7a,12a)-2-(3-methoxyphenyl)-2-oxoethyl ester-7,12-dihydroxy-cholan-24-oic acid	C33 H48 O6	1
Cpd 86: Norrubrofusarin 6-beta-gentiobioside	18.172	582.1513	31412	Norrubrofusarin 6-betagentiobioside	C26 H30 O15	2
Cpd 87: 18.382	18.382		40511			
Cpd 88: 5,6:8,9-Diepoxyergost-22-ene-3,7beta-diol	18.426	444.326		5,6:8,9-Diepoxyergost-22-ene-3,7beta-diol	C28 H44 O4	5
Cpd 89: (24E)-15alpha-Acetoxy-3alpha-hydroxy-23-oxo-7,9 (11),24-lanostatrien-26-oic acid	18.455	526.3322	146433	(24E)-15alpha-Acetoxy-3alphahydroxy-23-oxo-7,9 (11),24-lanostatrien-26-oic acid	C32 H46 O6	2
Cpd 90: (5b,7a,12a)-2-(3-methoxyphenyl)-2-oxoethyl ester-7,12-dihydroxy-cholan-24-oic acid	18.642	540.3477	144409	(5b,7a,12a)-2-(3-methoxyphenyl)-2-oxoethyl ester-7,12-dihydroxy-cholan-24-oic acid	C33 H48 O6	1
Cpd 91: Assafoetidin	18.804	382.217		Assafoetidin	C24 H30 O4	10
Cpd 92: 18.889	18.889		111038			
Cpd 93: 19.140	19.14					
Cpd 94: Euphornin	19.149	584.3021	17951	Euphornin	C33 H44 O9	2
Cpd 95: 7b-Hydroxy-3-oxo-5b-cholanoic acid	19.369	390.2776		7b-Hydroxy-3-oxo-5b-cholanoic acid	C24 H38 O4	10
Cpd 96: Propaquizafop	19.51	443.1203		Propaquizafop	C22 H22 Cl N3 O5	1
Cpd 97: 19.687	19.687					
Cpd 98: 7b-Hydroxy-3-oxo-5b-cholanoic acid	19.718	390.2778		7b-Hydroxy-3-oxo-5b-cholanoic acid	C24 H38 O4	10
Cpd 99: Temocaprilat	20.24	448.1157		Temocaprilat	C21 H24 N2 O5 S2	1
Cpd 100: 26.684	26.684					

Table 2b1: Molecular docking values of active compounds with protein AR (2AMA).

Ligand	Affinity (kcal/mol)	H-bonds	H-bond length (Å)	H-bond with	Hydrophobic interactions
MF1	−7.2	2	2.81	2AMA:Arg752::MF1:O6	Leu701, Leu704, Asn705, Leu707, Gly708, Trp741, Met742, Met745, Val746, Met749, Met780, Met895
			3.06	2AMA:Phe764::MF1:O6	
MF4	−6.0	2	3.03	2AMA:Leu704::MF4:O	Leu701, Gly708, Met742, Met745, Val746, Phe764, Met780, Met787, Leu873, Thr877, Met895
			3.09	2AMA:Asn705::MF4:O	
MF6	−6.9	4	2.96	2AMA:Ser703::MF6:O3	Ser702, Glu706, His689, Ala699, Asp890, Pro892
			3.04	2AMA:Phe891::MF6:O2	
			3.10	2AMA:Gly688::MF6:O3	
			3.26	2AMA:Asp690::MF6:O3	
DICLOFENAC	−7.6	1	3.01	2AMA:Thr877::DIC:O1	Leu704, Leu707, Gly708, Trp741, Met742, Met745, Val746, Met749, Arg752, Phe764, Met780, Met895

Table 2b2: Molecular docking values of active compounds with protein ESR1 (1A52).

Ligand	Affinity (kcal/mol)	H-bonds	H-bond length (Å)	H-bond with	Hydrophobic interactions
MF1	−7.9	1	2.97	1A52:Leu387::MF1:O6	Leu346, Leu349, Ala350, Glu353, Trp383, Leu384, Leu391, Phe404, Gly521, Leu525
MF4	−7.1	1	2.99	1A52:Thr347::MF4:O	Leu346, Ala350, Trp383, Leu384, Leu387, Met388, Met421, Ile424, Gly521, His524, Leu525
MF6	−7.0	1	2.99	1A52:Ser512::MF6:O2	Ile451, Asn455, Tyr459, Leu479, Thr483, Leu508
DICLOFENAC	−8.4	1	2.85	1A52:Thr347::DIC:O2	Met343, Leu346, Ala350, Leu384, Leu387, Phe404, Ile424, Gly521, His524, Leu525

Table 2b3: Molecular docking values of active compounds with protein CYP19A1 (3EQM).

Ligand	Affinity (kcal/mol)	H-bonds	H-bond length (Å)	H-bond with	Hydrophobic interactions
MF1	−8.1	2	2.72	3EQM:Asp309::MF1:O6	Arg192, Phe221, Asp222, Gln225, Val313, Ile474, His480, Glu483
			2.88	3EQM:Gln218::MF1:O4	
MF4	−5.2	2	2.75	3EQM:Glu483::MF4:O	Arg192, Phe221, Asp222, Ile474, His480, Asp482, Thr484
			2.80	3EQM:Gln218::MF4:O	
MF6	−7.0	3	2.70	3EQM:Gln218::MF6:O3	Val215, Lys216, Gly219, Lys246, Asp250
			2.96	3EQM:Lys243::MF6:O2	
			3.04	3EQM:Ser247::MF6:O2	
DICLOFENAC	−5.7	2	2.89	3EQM:Gln225::DIC:O1	Gln218, Phe221, Asp222, Ile474, Glu483, Thr484
			2.97	3EQM:His480::DIC:O1	

Table 2b4: Molecular docking values of active compounds with protein RARA (2A9E).

Ligand	Affinity (kcal/mol)	H-bonds	H-bond length (Å)	H-bond with	Hydrophobic interactions
MF1	−8.3	3	2.86	2A9E:Leu202::MF1:O5	Ala201, Cys274, Thr275, Leu316, Leu317, Met321, Asp323, Thr326
			3.18	2A9E:His195::MF1:O6	
			3.18	2A9E:Tyr277::MF1:O2	
MF4	−7.6	1	2.79	2A9E:Ser232::MF4:O	Phe228, Leu266, Leu269, Ile270, Phe302, Leu305, Val309, Gly391, Val395, Leu414
MF6	−6.9	3	2.68	2A9E:Met43::MF6:O2	Ala263, Arg339, Ser388, Ala389, Ala392, Leu414, Glu415
			3.14	2A9E:Arg385::MF6:O3	
			3.30	2A9E:Lys262::MF6:O2	
DICLOFENAC	−7.3	1	2.88	2A9E:Ser232::DIC:O2	Phe228, Leu269, Ile270, Gly301, Phe302, Leu305, Arg394, Leu398, Ile410, Leu414

Table 2b5: Molecular docking values of active compounds with protein TSHR (3G04).

Ligand	Affinity (kcal/mol)	H-bonds	H-bond length (Å)	H-bond with	Hydrophobic interactions
MF1	−6.9	4	2.92	3G04:Pro142::MF1:O6	Met140, Asp143, Ser166, Pro168, Val169
			3.04	3G04:Ala171::MF1:O6	
			3.30	3G04:Leu144::MF1:O6	
			3.33	3G04:Phe141::MF1:O2	
MF4	−5.2	2	2.79	3G04:Pro142::MF4:O	Asp143, Thr145, Pro168, Val169, Asn170
			2.94	3G04:Phe141::MF4:O	
MF6	−5.7	2	2.87	3G04:Glu247::MF6:O2	Gly223, Val224, Tyr225, Lys244, Gly245, His248
			3.10	3G04:Leu246::MF6:O2	
DICLOFENAC	−5.7	2	2.70	3G04:Thr145::DIC:O2	Asp143, Pro168, Val169, Asn170, Ala171
			3.07	3G04:Leu144::DIC:O2	

Table 2b6: Molecular docking values of active compounds with protein NFKB1 (1SVC).

Ligand	Affinity (kcal/mol)	H-bonds	H-bond length (Å)	H-bond with	Hydrophobic interactions
MF1	−6.3	2	2.78	1SVC:Ser81::MF1:O3	Lys52, Gly55, Phe56, Gly68, Gly69, Pro71, Gly72, Ser74, Lys80,
			2.83	1SVC:Ser81::MF1:O2	
MF4	−4.9	2	3.06	1SVC:Lys79::MF4:O	Lys52, Gly69, Pro71, Gly72, Ser74, Lys80
			3.15	1SVC:Ser81::MF4:O	
MF6	−6.6	4	2.91	1SVC:Ser74::MF6:O3	Lys52, Phe56, His67, Gly68, Gly69, Pro71, Ser75
			3.15	1SVC:Lys79::MF6:O3	
			3.15	1SVC:Gly55::MF6:O2	
			3.31	1SVC:Ser81::MF6:O3	
DICLOFENAC	−5.6	1	2.99	1SVC:Ser113::DIC:O2	Val61, Asp121, Leu143, Val145, Thr153, Ala156, Arg157

Table 2b7: Molecular docking values of active compounds with protein ALB (1H9Z).

Ligand	Affinity (kcal/mol)	H-bonds	H-bond length (Å)	H-bond with	Hydrophobic interactions
MF1	−7.8	3	2.89	1H9Z:Arg218::MF1:O1	Glu294, Tyr341, Ser342, Val343, Lys444, Pro447, Glu450, Asp451
			3.11	1H9Z:Asn295::MF1:O6	
			3.33	1H9Z:Gln221::MF1:O3	
MF4	−6.4	1	3.17	1H9Z:His242::MF4:O	Trp214, Arg218, Leu219, Arg222, Leu238, Ile264, Ile290, Ala291
MF6	−9.2	2	2.75	1H9Z:Arg257::MF6:O3	Glu153, Lys195, Leu198, Lys199, Phe211, Trp214, His242, Ala291
			3.28	1H9Z:Ser454::MF6:O2	
DICLOFENAC	−7.7	1	2.91	1H9Z:Ser454::DIC:O1	Lys199, Leu198, Trp214, Glu450, Asp451, Leu481

ALB: Albumin.

Supplementary Figures

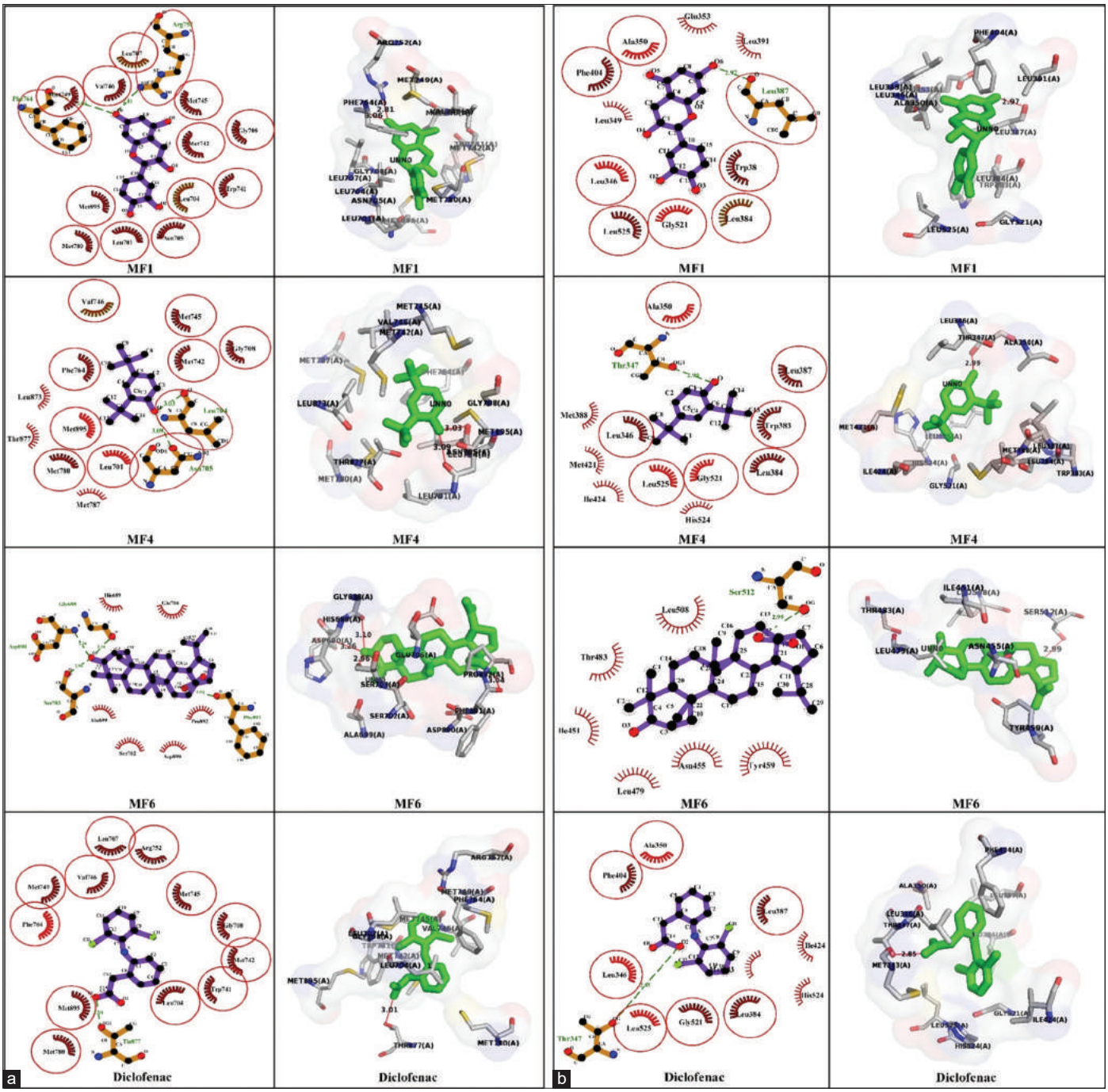

Figure 1: (a) The molecular docking results of active compounds against AR protein, represented in both 2D and 3D. (b) The molecular docking results of active compounds against TSHR protein, represented in both 2D and 3D.

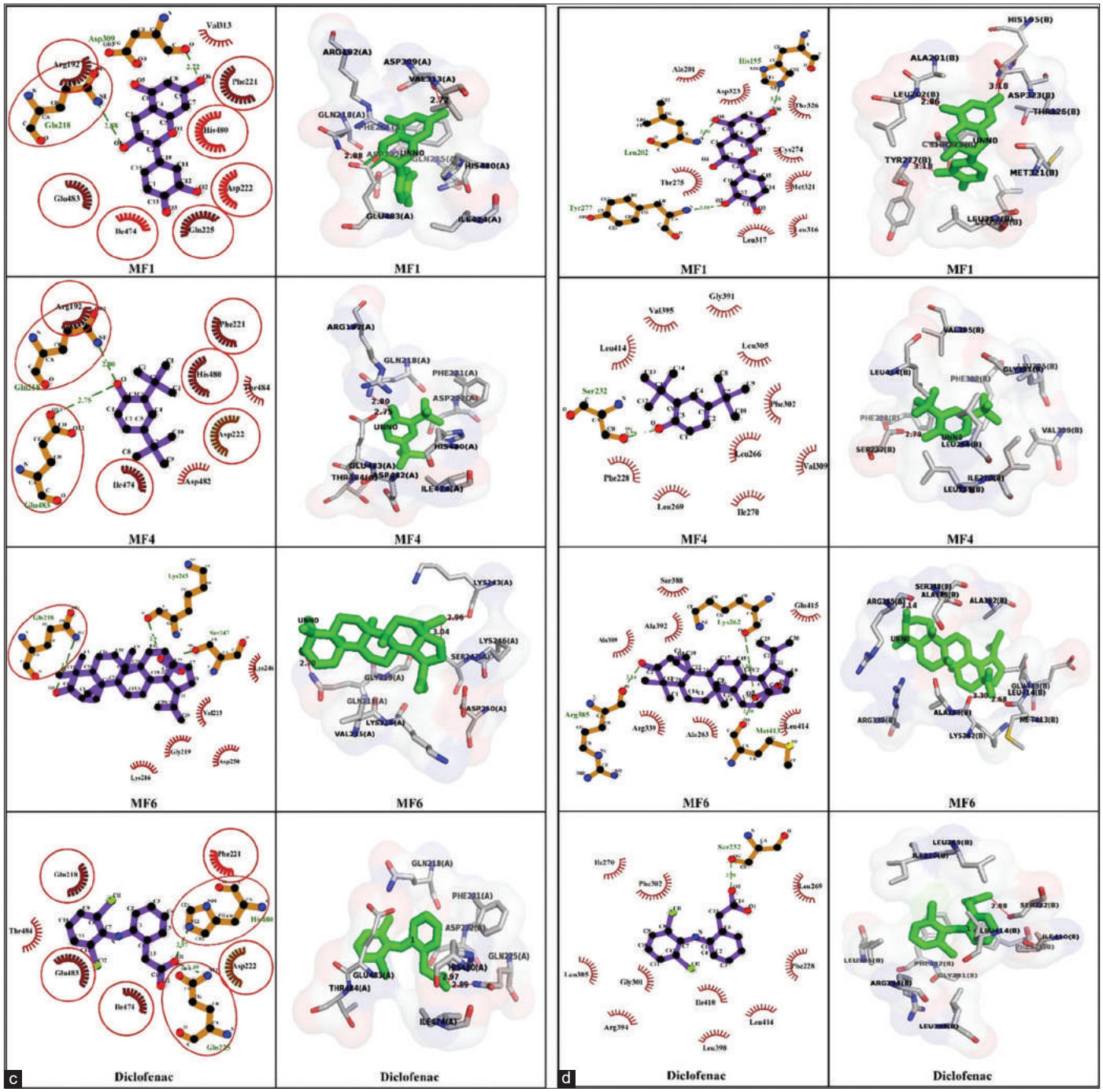

Figure 1: (c) The molecular docking results of active compounds against CYP19A1 protein, represented in both 2D and 3D. (d) The molecular docking results of active compounds against RARA protein, represented in both 2D and 3D.

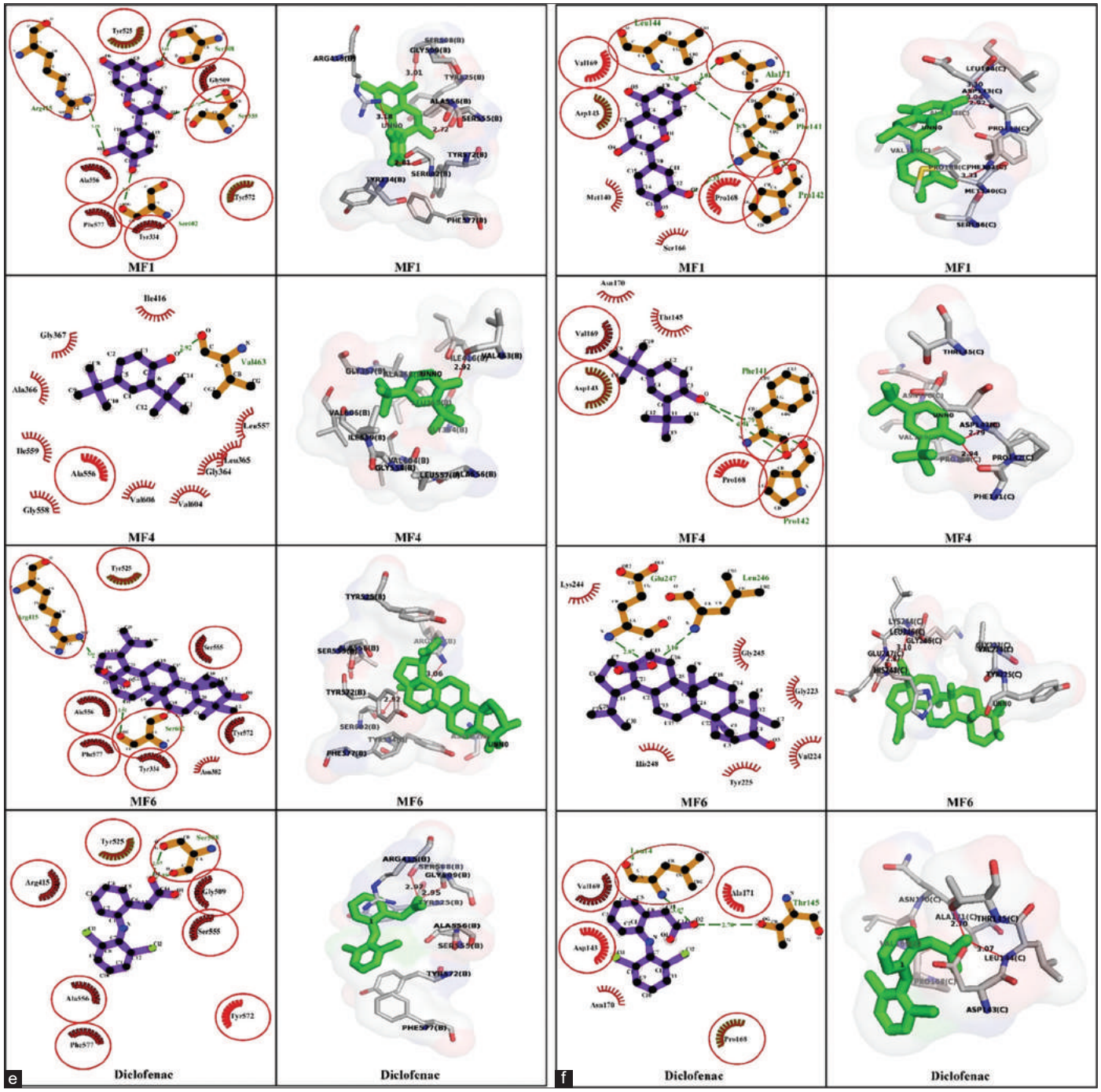

Figure 1: (e) The molecular docking results of active compounds against NFE2L2 protein, represented in both 2D and 3D. (f) The molecular docking results of active compounds against TSHR protein, represented in both 2D and 3D.

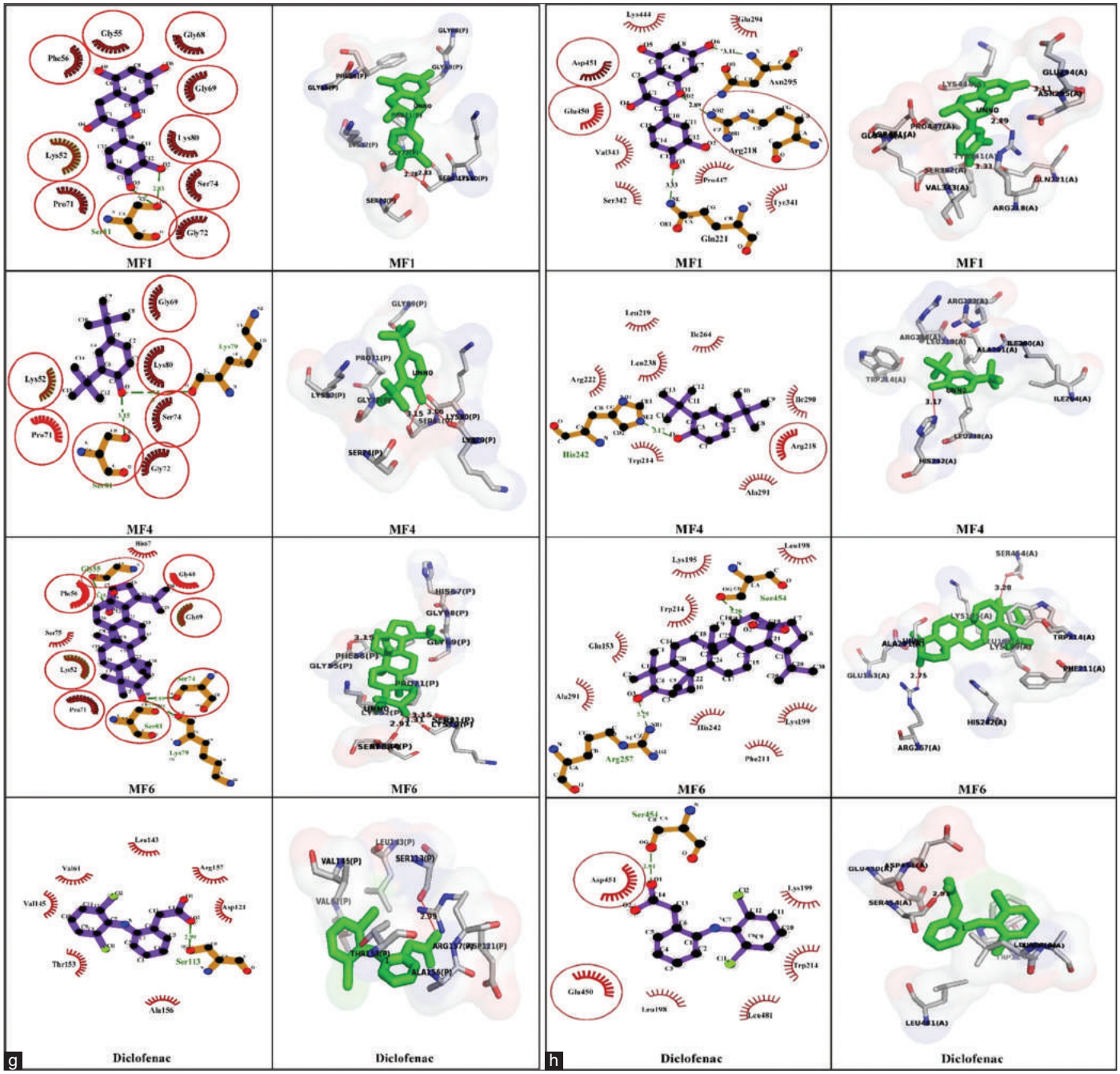

Figure 1: (g) The molecular docking results of active compounds against NFKB1 protein, represented in both 2D and 3D. (h) The molecular docking results of active compounds against ALB protein, represented in both 2D and 3D.